AGU Books

Rare Earth Elements in Coal-combustion Fly Ash and Their Potential Recovery

Journal:	*AGU Books*
Manuscript ID	2020-Nov-CH-1311.R1
Wiley - Manuscript type:	Chapter
Date Submitted by the Author:	n/a
Complete List of Authors:	Hower, James; University of Kentucky, Center for Applied Energy Research Kolker, Allan; U.S. Geological Survey, Geology, Energy, and Minerals Science Center Hsu-Kim, Heileen; Duke University, Department of Civil & Environmental Engineering Plata, Desirée; Massachusetts Institute of Technology, Department of Civil & Environmental Engineering
Primary Index Term:	210 - Coal Geology < 200 - GEOHEALTH
Index Term 1:	215 - Economic geology < 200 - GEOHEALTH
Index Term 2:	3625 - Petrography, microstructures, and textures < 3600 - MINERALOGY AND PETROLOGY
Index Term 3:	6699 - General or miscellaneous < 6600 - PUBLIC ISSUES
Index Term 4:	1065 - Major and trace element geochemistry < 1000 - GEOCHEMISTRY
Keywords:	lanthanides, recovery, mineral processing, coal, fly ash
Abstract:	Coal fly ash has long been considered a potential resource for recovery of valuable elements, such as rare earth elements (REE), which are retained and concentrated upon combustion of coal feedstocks. Understanding REE occurrence within fly ash is a key to developing possible recovery methods. Recent results using modern analytical approaches shed light on the distribution REE in fly ash and the approaches required for their recovery. Some of the highest REE contents occur in fly ash derived from U.S. Appalachian Basin coals, and among these, coals influenced by input volcanic ash (Fire Clay coal, Kentucky) are especially enriched. Leaching studies of bulk fly ash show that, as a proportion of the total REE present, samples from eastern U.S. coals are generally less readily extractible than fly ash derived from western U.S. coals having lower REE contents. Direct determinations by ion microprobe show that REE in a range of fly ash samples are partitioned into aluminosilicate glasses formed during melting at boiler temperatures. These glasses comprise the largest mass fraction of coal fly ash. REE-enriched domains are present locally in fly ash at the nanometer scale (as shown by TEM), and these REE coexist with the

	glass phase. To enable systematic study of these REE, Ce has been proposed as a proxy for the trivalent lanthanides, as supported by speciation determinations demonstrating that Ce occurs in the trivalent form in fly ash. Despite a decreasing proportion of coal use for electric power generation in the U.S. and elsewhere, annual fly ash production, combined with coal ash already in storage, make up a large resource for potential recovery of rare earths and associated critical elements. Further developments in extraction technologies are needed to overcome difficulties in REE concentration and purification to produce REE materials of saleable purity derived from coal ash.

Rare Earth Elements in Coal Fly Ash and their Potential Recovery

James C. Hower

Center for Applied Energy Research, University of Kentucky, Lexington, Kentucky, USA (1-859-257-0261; james.hower@uky.edu)

Allan Kolker

Geology, Energy, & Minerals Science Center, U.S. Geological Survey Reston, Virginia, USA (akolker@usgs.gov)

Heileen Hsu-Kim

Department of Civil & Environmental Engineering, Duke University, Durham, North Carolina, USA (hsukim@duke.edu)

Desirée L. Plata

Department of Civil & Environmental Engineering, Massachusetts Institute of Technology, Cambridge, Massachusetts, USA (dplata@mit.edu)

Abstract

Coal fly ash has long been considered a potential resource for recovery of valuable elements, such as rare earth elements (REE), which are retained and concentrated upon combustion of coal feedstocks. Understanding REE occurrence within fly ash is a key to developing possible recovery methods. Recent results using modern analytical approaches shed light on the distribution REE in fly ash and the approaches required for their recovery. Some of the highest REE contents occur in fly ash derived from U.S. Appalachian Basin coals, and among these, coals influenced by input volcanic ash (Fire Clay coal, Kentucky) are especially enriched. Leaching studies of bulk fly ash show that, as a proportion of the total REE present, samples

from eastern U.S. coals are generally less readily extractible than fly ash derived from western U.S. coals having lower REE contents. Direct determinations by ion microprobe show that REE in a range of fly ash samples are partitioned into aluminosilicate glasses formed during melting at boiler temperatures. These glasses comprise the largest mass fraction of coal fly ash. REE-enriched domains are present locally in fly ash at the nanometer scale (as shown by TEM), and these REE coexist with the glass phase. To enable systematic study of these REE, Ce has been proposed as a proxy for the trivalent lanthanides, as supported by speciation determinations demonstrating that Ce occurs in the trivalent form in fly ash. Despite a decreasing proportion of coal use for electric power generation in the U.S. and elsewhere, annual fly ash production, combined with coal ash already in storage, make up a large resource for potential recovery of rare earths and associated critical elements. Further developments in extraction technologies are needed to overcome difficulties in REE concentration and purification to produce REE materials of saleable purity derived from coal ash.

1. INTRODUCTION

Rare earth elements (REEs) are critical in the production of a wide array of electronics, magnets, catalysts, metal alloys, optics, and other items needed in modern society (Greene, 2012; Hatch, 2012; Dobransky, 2013; U.S. Geological Survey, 2014; Basu, 2017; Watson, 2018; Home, 2020). Coal, coal waste, and coal combustion products make up one of the most actively investigated categories of secondary sources for potential REE recovery (U.S. Department of Energy, 2018). Coal use currently accounts for about 30 percent of the electric power generated in the United States (Energy Information Administration (EIA), 2018). Fly ash, produced during the burning of coal, is a fine-grained solid derived from non-combustible mineral constituents of

coal. Coal combustion results in the retention and enrichment of REEs in fly ash (Clarke and Sloss, 1992; Ratafia-Brown, 1994). As a result, fly ash has long been considered a potential resource for recovery of REEs and other valuable elements (Goldschmidt, 1935; Seredin and Dai, 2012). The United States has the world's largest coal reserves (World Energy Council, 2016). World coal consumption for power generation is projected to increase from 2017 to 2040, with reductions in the US, the European Union, and Japan offset by more-or-less steady trends in China and increases in coal-fired generation in India (International Energy Agency, 2018; Patel, 2019; Kaplan, 2020). Even as gas-fired power generation has increased significantly in the last decade, production of vast quantities of fly ash has continued. Advanced power generation systems will account for some of the growth in coal-fired power generation, resulting in greater generating efficiency, implying about 1/3rd less coal will be required per MWh of generation (Sloss, 2019). About 55.5% of the 36.2 Mt of fly ash produced annually in the U.S. is beneficially reused (2018 data; American Coal Ash Association, 2019). The remainder is stored, mostly in landfills and impoundments. Thus, annual fly ash production, combined with fly ash already in storage, constitutes a huge potential resource (Hower et al., 2017b). For example, the annual production of the unused (and presumably discarded) portion of coal fly ash in the U.S. comprises a REE reserve that is similar in scale to the the Mountain Pass mine (Taggart et al., 2016). Of coal-related materials investigated for potential REE recovery, fly ash has among the highest REE contents, and due to its fine grain size, ostensibly requiring minimal processing compared to mining and extraction of conventional REE ores. Viable and sustainable recovery of REE from fly ash greatly depends on geochemical and physical properties of the ash matrix.

1.1 Nature of Fly Ash

During coal combustion for electric power generation, the inorganic constituents in the parent coal experience a variety of processes at boiler temperatures (1300-1600 °C) that largely govern the geochemical properties of fly ash collected from the flue gas. Clay minerals in coal melt to form a glass (i.e., an amorphous solid); quartz undergoes a phase transformation to the high-temperature β form, eventually becoming β cristobalite; and pyrite is oxidized to iron oxides (Ward and French, 2006; Kutchko and Kim, 2006; Hower, 2012; Kolker, 2018). Melting temperatures of some of the most common REE-bearing minerals in coal, such as zircon and monazite, are higher than the boiler temperatures and, as a result, these trace phases should survive the combustion process. However, these phases are commonly dispersed throughout the fly ash matrix compared to their distribution in the feed coal (Section 2.2). In addition to the phase transformation of parent minerals, new (neoformed) minerals, such as mullite ($Al_6Si_2O_{13}$), form by high-temperature reactions in the boiler. Glass formed by quenching of the melt is the most abundant constituent of fly ash.

Classification of coal ash is based on its major element characteristics expressed as the sum of $SiO_2 + Al_2O_3 + Fe_2O_3$ compared to other major constituents. "Cementitious" ash is classified as Class C where $SiO_2 + Al_2O_3 + Fe_2O_3$ is greater than or equal to 50 weight percent. For fly ashes with the sum of these constituents greater than or equal to 70 weight percent, the "pozzolanic" ash is classified as Class F (ASTM International, 2017). Each classification has specific properties for use in concrete. Other beneficial reuses of coal fly ash include structural fill and other construction materials (American Coal Ash Association, 2019). Unused ash is stored as solid waste, often in landfills or surface water impoundments located adjacent to coal fired power plants. In the U.S., a ruling by the Environmental Protection Agency (EPA, 2014) upheld the "nonhazardous" classification for fly ash while also recommending improved

monitoring of existing disposal impoundments. This policy allows for continued beneficial use of coal fly ash in construction materials and in other applications, while also encouraging exploration of new reuse opportunities (EPA, 2014).

1.2 *REE in Coal and Coal Ash*

The International Union of Pure and Applied Chemistry (IUPAC; Connelly et al. 2005) defines the rare earth metals as the lanthanides, plus scandium (Sc) and yttrium (Y). Apart from literature referring to other nomenclature, the REE designation for the lanthanides, Y, and Sc, as per Connelly et al. (2005) is followed here. The lanthanide series and its range in atomic number from 57 to 71 results from progressive filling of 4f valence electron orbitals; lanthanum (La, atomic number 57) does not have 4f electrons, whereas Lutetium (Lu, atomic number 71) has fourteen and a full 4f level. As such, the 15 elements of the lanthanide series exhibit a continuous distribution of chemical and physical properties (e.g., atomic radii). Nonetheless, various classification approaches have been introduced to understand similarities and differences among the elements in the series. Traditionally, the lanthanides are divided into light, middle, and heavy rare earths (Hanson, 1980). For some studies involving coal, the series has been divided only into light rare earth elements (LREE; La to Sm) and heavy rare earth elements (HREE; Eu to Lu), with Y sometimes included among the HREE (Seredin, 1996; Hower et al., 1999, 2016a; Mardon and Hower, 2004; Dai et al., 2016b; Lin et al., 2017a; among others). Others have used the LREE/HREE ratio in evaluations of REE distribution in coal and coal products (Seredin, 1996; Balashov, 1976). In other coal-related studies, REY (lanthanides + Y) have been divided into light, medium, and heavy fractions: LREY (La through Sm), MREY (Eu through Dy plus Y), and HREY (Ho through Lu). Following normalization of REE abundances to crustal averages (indicated here by the suffix "N"), further delineation can be made of L-type

(light type; $La_N/Lu_N > 1$), M-type (medium type; $La_N/Sm_N < 1$, $Gd_N/Lu_N > 1$), and H-type (heavy type; $La_N/Lu_N < 1$) enrichment patterns (Seredin and Dai, 2012).

The concentration of REE in fly ashes from three US coal basins was shown by Taggart et al. (2016, their Fig. 2). The ash-basis concentrations in the coal are similar to the ash-basis concentrations in the resulting fly ashes. For the samples discussed by Taggart et al., Central Appalachian Basin-derived fly ashes had the highest REE concentration followed by Illinois Basin- and Powder River Basin-derived fly ashes. Normalization of the REE series facilitates observations of enrichments or depletions relative to natural abundances, which display a sawtooth pattern where elements with even atomic numbers are more abundant than their nearest odd-numbered neighbors (Figure 1A). This pattern reflects the Oddo-Harkins effect, in which elements with even atomic numbers are more abundant in the universe than odd-numbered elements due to the enhanced stability of nuclei with spin-paired protons (i.e., an even number of protons: Oddo, 1914; Harkins, 1917). To more easily compare the REE abundance distribution of different samples and eliminate the sawtooth pattern resulting from the Oddo-Harkins effect, REE are commonly "normalized" by dividing by a reference such as the REE content of the upper continental crust (UCC; Figure 1B), or by that of chondrites, a group of stony meteorites (Figure 1C). Chondrites were chosen by geochemists because they are among the most primitive materials in the solar system, and therefore, approximate the bulk Earth prior to its differentiation into a core, mantle, and crust. Relative to chondrites, the upper continental crust is enriched with light REEs, and most coals show a similar crustal REE distribution. This distribution pattern is retained during coal combustion, but with overall enrichment (Figure 1) or concentration. Besides normalization to UCC or to chondrites, in some REE studies, normalization to shale composites such as the North American Shale Composite (NASC; Gromet

et al., 1984) have been used. In presenting REE data, any of these standard normalization approaches are acceptable.

The inclusion of Y and Sc in many REE studies is motivated by their industrial utility rather than some geochemical motivation; Sc is seldom found in the same minerals as the other REEs. However, owing to the price commanded for Sc, several U.S.-based coal- and coal-combustion fly-ash-based projects are relying on the co-extraction and concentration of Sc in order to underwrite the economics of their projects (Wraich, 2017). This is challenging because Sc exhibits a distinct behavior from the lanthanides, which behave similarly as a group, largely due to their common occurrence and trivalent form and similar ionic radii, with Y fitting in with the heavy REE. Exceptions include Ce and Eu, which may also exist in tetravalent and divalent forms, respectively. As such, Ce and Eu are, in some cases, fractionated from the trivalent lanthanides under certain redox conditions (Hanson, 1980). This fractionation results in so-called anomalies, where the content of a single element diverges from the smooth pattern defined for all the remaining trivalent lanthanides on normalized plots. Europium commonly shows such anomalies on chondrite-normalized plots but these may be absent in UCC-normalized plots because a negative europium anomaly (relative to chondrites) is inherent in the crustal distribution (Figure1c). Surprisingly, in certain coals with UCC-normalization, similar anomalies have been shown for non-redox sensitive trivalent-only lanthanides such as Gd (Dai et al, 2016a). If present in feed coals, such anomalous lanthanide distributions would be retained by the ash during coal combustion.

REE-bearing minerals in coals include major constituents such as clays, carbonates, and phosphate minerals, as well as REE trace phases such as monazite ((Ce, La, Nd, Th) PO_4), allanite ($(Ce,Ca,Y)_2$ $(Al,Fe^{3+})_3$ $(SiO_4)_3$ (OH)), zircon ($ZrSiO_4$), and xenotime (YPO_4; Finkelman,

1981). Additional REE minerals reported in some coals include rhabdophane ((Ce, La, Y) PO_4• H_2O) (Dai et al., 2014a), florencite ($CeAl_3(PO_4)_2(OH)_6$) (Hower et al, 2020a), and Ce-Nd-bearing carbonates (Dai et al., 2016b, 2017; Zhao et al., 2017). Organic-hosted REE are also indicated, especially for the heavy rare earths (Eskanazy, 1987a, b; 1999).

In some cases, REE minerals present in coal have been shown to survive combustion. For example, during combustion of Polish hard coal in the Upper Silesian region, Smolka-Danielowska (2010) found that monazite, zircon, and xenotime remained in fly ash following combustion at unspecified conditions. In a combined X-ray diffraction (XRD) and scanning electron microscopy (SEM) study, Brownfield et al. (1999, 2005) found REE-bearing minerals (zircon, apatite, and monazite) were retained in the fly ash and bottom ash from the burning of a Powder River Basin, Wyoming, coal. An unidentified REE-bearing Ca-P-silicate was also found in the fly ash (Brownfield et al., 2005; their Figure 30). As noted above, REE-bearing minerals are more dispersed in fly ash than in the respective feed coal (section 2.2), despite the relative enrichment of REE in fly ash. In SEM examination of a Kentucky coal and its corresponding ash, Zhang et al. (2015) found that REE-bearing trace phases were more apparent in the coal and the separation of trace phases from the ash did not result in increased REE contents in the trace mineral fraction, suggesting that these trace phases were not the primary mode of REE occurrence.

1.3 Trends in Coal Production and Use

REE contents and composition in fly ash depend greatly on the parent coal feedstock. Thus, the amount and type of coal burned for electricity have considerable implications for the quantity and quality of the REE reserves in fly ash. In the U.S., coal production and the proportion of coal-based electric power generation has been declining since 2011. Houser et al.

(2017) noted three primary reasons for the decline in the U.S.: (1) a decline in the consumption of electricity, with the 2016 consumption being less than in 2007 in spite of a larger economy; (2) the rapid increase in production of shale gas, resulting in a 70% decrease in the price of natural gas from 2008 to 2016 (in 2016 dollars); and (3) the incursion of wind- and solar-powered power generation into the previously coal-dominated market. Of these, the supply, low price, and price stability of natural gas dominated the transition away from coal-fired power generation. In addition to these factors, in some coalfields, particularly in the Appalachians, the impact of declining coal reserves and a general decrease in quality and thickness of the remaining reserves has led to a striking increase in the cost of mining and processing coal. As an example of a cost factor, the average amount of land surface required to extract each ton of coal mined in eastern Kentucky tripled from 2008 to 2015 (Wright, 2018).

The decline in coal-fired power generation versus the corresponding rise in gas-fired generation is reflected in a doubling of the U.S. gas capacity and a halving of the coal capacity from 2015 to 2017, with each accounting for about 85-90 million MWh/year of generation by 2017 (Hoff, 2017). The decline in coal-fired generation has also triggered other major operational changes, such as conversion of generation stations to natural gas, modifications to another coal source, or retirement/closure of power plants. For plants previously burning low-S Central Appalachian coal, such a switch has often been to high-S Illinois Basin coal because (1) it is substantially cheaper ($34.00/short ton vs. $56.90/short ton, for the week ending 12 June 2020, where a short ton is a U.S. ton, equivalent to 907.19 kg or 2,000 lbs,; EIA, 2020) and (2) with the implementation of revised SO_2-emission and Hg-control standards (EPA, 2019, 2020) and the need to install some form of emission-control system, the choice of high-S coal became viable. Overall, 43 GW of coal-fired capacity was retired from 2012 to 2017, and this was

somewhat offset by efficiencies of new coal-fired units; new units had a heat rate of 10,197 kJ/kWh compared to 10,912 kJ/kWh for the retired units, an added efficiency equivalent to 19.45 GW of capacity (EIA, 2017).

As an example of the cumulative impact of the factors noted above, of the 58 power plants burning Central Appalachian coal in 10 eastern U.S. states in 2008 (information from Keystone Coal Industry Manual, 2009), roughly 22 were still using Central Appalachian coal in 2018 (based on personal knowledge and checks of publicly available information by the first author). Since Central Appalachian coals, particularly those from eastern Kentucky, have some of the best prospects for REE recovery among eastern U.S. coals (Hower et al., 1999, 2016b, 2020b; Mardon and Hower, 2004; Lin et al., 2018a), the proportionately large decrease in Central Appalachian-sourced coal means that active production of some of the inherently highest-REE-concentration (e.g., those derived from the Fire Clay coal) fly ashes has diminished. Discussions of the geology of REE incorporation and occurrence in coal are out of the scope of this chapter; global observations by Seredin and Dai (2012) and Appalachian-centered discussions by Hower et al. (2016b, 2020c) cover aspects of the subject. Overall, the decrease in coal-fired generating capacity implies a decrease in the amount of fly ash being generated, from 78.454 Mt in 2008 to 36.2 Mt in 2017 (American Coal Ash Association, 2019). The long history of use of such coals, though, means that much of the ash generated over decades of coal utilization remains in pond or landfill storage throughout a large portion of the U.S., but environmental and regulatory factors for recovering this material have not been addressed. Altogether, the coal power and coal ash industries continue to change at a rapid pace, and this evolution will alter the outlook for fly ash as an unconventional REE resource.

1.4 Critical Elements and U.S. Fly Ash Resources

Critical materials are defined as those that are essential to the economy but whose supply might be limited (Neuendorf et al., 2005). Apart from inclusion of all REE among a group of 35 elements deemed critical to the U.S. (Fortier el al., 2018),division among REE into critical (Nd, Eu, Tb, Dy, Y, and Er), uncritical (La, Pr, Sm, and Gd), and excessive (Ce, Ho, Tm, Yb, and Lu) groups (after Seredin, 2010; Seredin and Dai, 2012) is somewhat subjective and transient, contingent upon the current demands of the market and the supplies on hand (Hatch, 2012). For example, Nd and Pr are in demand (in 2018) for use in permanent magnets with Dy used to increase the performance of the magnets in high-T environments (Roskill, 2017, 2018). Potentially economic levels of REEs occur in many U.S. coals (data from Bragg et al., 1998; Palmer et al., 2015). However, because most coals and coal fly ashes are LREE-enriched, and the most abundant elements of the LREE (La and Ce) are not in the critical category, the proportion of critical elements is limited to about 45% of the total REE (using the classification of Seredin (2010) and Seredin and Dai (2012)). Nevertheless, a mix of elements tending towards the less-valuable uncritical and excessive categories can directly influence the economics of a mining or processing operation (Miller, 2015). Most of the REE mining and processing has been concentrated in China, and even newer, non-Chinese operations turn to the Chinese market for processing and downstream manufacturing (Merriman and Backeberg, 2018).

2. GEOCHEMICAL CHARACTERIZATION OF FLY ASH

Knowledge of the geochemical distribution of REE in coal or fly ash can inform REE recovery strategies. Primary approaches to determine targeted REE mineral hosts in devising REE recovery strategies include extraction of bulk samples using a variety of techniques; elemental analysis methods, such as inductively coupled plasma mass spectrometry (ICP-MS); and grain-scale trace element microanalysis using either laser ablation or ion microprobe approaches.

Speciation of relatively abundant REE such as Ce can be accomplished using synchrotron-based X-ray absorption near-edge structure (XANES) on either the bulk- or micro-scale. Transmission electron microscopy (TEM) is useful in characterizing nanometer-scale REE-bearing domains, which may differ considerably from macro- and micro-scale REE hosts. We detail some of the major findings of these efforts in the following discussion.

2.1 Bulk Characterization of Rare Earth Elemental Contents via ICP-MS

The determination of trace element contents in coal fly ash generally requires a combination of robust methods to solubilize the target analytes from the ash followed by sensitive detection methods that can accommodate the matrix complexity of the digests.

For the analysis of REEs, the elements must first be liberated from the particles into an aqueous solution phase. Because these elements are mostly encapsulated within aluminosilicate glasses of fly ash particles and, further, can be difficult to dissolve, the extraction step generally require reagents that can decompose this matrix. Common leaching methods entail heated wet-digestion methods developed for geological materials, including heated acid digestion with HF alone or combined with other acids (e.g., HNO_3, H_2O_2, HCl, $HClO_4$,) (Lichte et al., 1987; Taggart et al., 2016). The acid mixture is then dried and re-dissolved in a dilute acid (e.g., HNO_3/HCl) that is compatible with the sample introduction system of analytical instrumentation. Alternatives to acid digestion which are more effective in breaking down insoluble REE-bearing trace phases such as zircon include flux fusion methods with lithium metaborate (Bank et al., 2016) and alkaline roasting with Na_2O_2 or NaOH (Taggart et al., 2018a).

The analysis of rare earth elements in the digestate solution requires highly sensitive analytical methods such as ICP-MS. Because rare earth elements can be prone to polyatomic interferences, especially for

complex matrices such as the acid leachates of coal fly ash, care must be taken to address such interferences. Collision or reaction cell technologies with a reaction gas (e.g., helium or hydrogen) for quadrupole ICP-MS can greatly reduce such polyatomic interferences and are now standard features in modern ICP-MS instrumentation. However, even with these improvements, other polyatomic interferences can greatly influence the accuracy of analysis for specific REE. For example, coal fly ash often contains large amounts of barium (Ba), resulting in $^{135}Ba^{16}O^{+}$ interference of the mass isotope signal for $^{151}Eu^{+}$. The correction for this interference has been addressed through a variety of approaches that include steps to remove Ba from the sample (Yan et al., 2018) or the use of high resolution mass spectrometry (Thompson et al., 2018). Other major constituents that might be relevant for digested coal fly ash include Ca, which interferes as $^{44}CaH^{+}$ with $^{45}Sc^{+}$, and oxide forms of light REE that have the same mass as heavy REE isotopes (Thomas, 2013).

Inductively coupled plasma optical emission spectrometry (ICP-OES) has also been used to determine REE. Hower et al. (2020b) discussed the comparisons between ICP-OES and ICP-MS, showing that there was a good correlation between the techniques for the more abundant REE but that ICP-MS was more suitable for the HREE, in particular, Tb and Ho through Lu.

2.2 Fly Ash and Bottom Ash Petrology

The various techniques for the examination of coal combustion ashes are all dependent on the scale of the investigation. Optical petrology is a valuable tool for the examination of plus-micron-size particles. The optical characterization of fly ash and bottom ash, typically done on polished, epoxy-bound particulate pellets (Hower, 2012; Suárez-Ruiz et al., 2017; Valentim, 2020), utilizes polarized reflected-light, oil-immersion optics in the analysis. While some studies, particularly for scanning electron microscopy, employ dispersed powder specimens

(Valentim et al., 2009), those types of preparations cannot match the petrographic detail seen in the cross sections of particles. In general, petrographic classifications of the ash are its coal maceral-derived constituents (including other organic-derived material such as biomass, petroleum coke, and tires), and inorganic-derived portions of the ash. In general, sub-micron particles cannot be seen or identified by optical microscopy.

Of the maceral-derived fly ash and bottom ash constituents, the products of the melting and repolymerization of bituminous vitrinite can be identified in both relatively unaltered inertinite and isotropic and anisotropic cokes (Figure 2 A&B). Also illustrated are the chars derived from lignite and subbituminous coals and anthracitic-vitrinite-derived carbons (Figure 2C&D).

The inorganic fly ash and bottom ash constituents include glass and glass with heated, but not melted, rock and carbon (Figure 3). As will be discussed below in this section and in section 2.6, fine-grained minerals, many of them below the resolution of optical petrology, can be enclosed within the glass. Spinel minerals (Figure 4), which include magnetite, are less abundant than glass, but can be common minerals in the combustion products of moderate- to high-pyrite coals. Spinels are often found within a glassy matrix. In both Figures 4B and 4C, note that some grains have a few-micron-thick red (hematite) oxidation rim. While such a feature would be a dominant feature in a powder-dispersion specimen, the views on the images shown here demonstrate that exploring only the surface conceals the rich variety of the interior of the particles. Mullite (Figure 5) is one of the neoformed minerals found in both fly ash and, more commonly, in bottom ash or stoker ash resulting from the combustion of high-Al-Si eastern U.S. bituminous coals. Mullite formation depends on the temperature and chemistry of the melt phase, with the mineral forming along with cristobalite during the cooling of an Al_2O_3-rich melt

in the Al_2O_3-CaO-SiO_2 system (Osborn and Muan, 1960; Ehlers, 1972; Alekseev and Vereshchagin, 1997). Increased concentrations of CaO in the melt, as would be common in the combustion of western U.S. low-rank coals, would result in the precipitation of neoformed anorthite from the melt (Hower et al., 2017c).

Although not common, optical microscopy reveals REE-minerals such as monazite in fly ash (Figures 6A and 6B). So, if monazite and other REE-rich minerals are rarely seen by optical microscopy, where are the REE in the fly ashes with over 1000 ppm REE? As the melting temperatures of pure phases of monazite (+/-2000 ºC) and zircon (1690 ºC) are well above normal combustion temperatures (1400-1500 ºC), it is not likely that there was much, if any melting of these minerals (Hikichi and Nomura, 1987; Finch and Hanchar, 2003; Seydoux-Guillaume et al., 2002; Quercia et al., 2007). Interestingly, Hood et al. (2017) demonstrated that monazite will shatter by 1400 ºC, well below its melting temperature, a mechanism attributed to the thermal expansion of helium, a product of the radioactive decay of the Th in the monazite (Farley, 2007; Cherniak et al., 2009; Cherniak and Watson, 2013; Guenthner et al., 2013).

In a study of sized fly ashes from the economizer, mechanical, and ESP rows at a power plant burning eastern US bituminous coal, Liu et al. (2017) demonstrated that the size-dependent variations in fly ash petrology influenced the distribution of the REE. Fly ash petrology and chemistry varies between the rows of the pollution control system, usually an array of a combination of economizer, cyclone (mechanical), electrostatic precipitator (ESP), and/or baghouse (fabric filter) units. Each successive row away from the boiler experiences a concomitant reduction in temperature and, usually, a decrease in the particle size of the ash (Hower et al., 2017c). Unlike volatile elements such as Zn or As, the concentration of REE

generally shows little variation between the progressive treatment rows, although the LREE/HREE ratio can vary (Hower et al., 2013b).

2.3 Trace element microanalysis

2.3.1 Laser-ablation ICP-MS \ and secondary ion mass spectrometry

Instrumentation for REE analysis on the scale of individual fly ash particles includes laser-ablation ICP-MS (LA-ICP-MS) and secondary ion mass spectrometry (SIMS; also called ion microprobe analysis). Each approach is discussed in detail elsewhere: for LA-ICP-MS these include Sylvester (2001, 2008) and Longerich (2008); for SIMS, these include Stern (2009), and Ireland (2014). This section will therefore emphasize cases with application of trace element microanalysis to coal ash. A fundamental difference in these microanalysis techniques is the rate and depth of penetration within the sample. In LA-ICP-MS, geologic samples are ablated to tens of micrometers in a matter of seconds. As a result, LA-ICP-MS is useful in studies of compositional variation with sample depth. In SIMS, a primary beam of incident ions sputters secondary ions from the sample at a much slower rate, typically leading to penetration depths of only about 1-5 micrometers, despite much longer analysis times. Compared to smaller ion microprobes, the SHRIMP-RG ion microprobe and other SHRIMP configurations (Section 2.3.2) employ a large format magnetic sector mass spectrometer with high mass resolution, thereby minimizing the effect of isobaric interferences in SIMS. In both LA-ICP-MS and SIMS, it is helpful to obtain standards that are homogenous on a grain scale and a good matrix match to the material being analyzed (Sylvester, 2001, 2008; Stern, 2009).

Early on, application of LA-ICP-MS to coal and coal ash focused on quantifying the distribution of elements of environmental interest, such as As and transition metals (Chenery et al., 1995; Querol and Chenery, 1995). In the fly ash study by Spears (2004), these also included

Pb, Se, Ga, and Ge). More recently, LA-ICP-MS has been used to map major and minor element distribution in fly ash particles (Bauer et al., 2017) and to compare results obtained by LA-ICP-MS to results by SEM-EDS (Piispanen et al., 2009) for major fly ash constituents such as Si, Al, Ca and Fe. Kostova et al. (2016) used LA-ICP-MS to determine bulk fly ash concentrations for a large range of elements by analyzing prepared fused glass discs of whole sample material. In a study of fly ash samples derived from the Fire Clay coal, Kentucky, Hood et al. (2017) used reconnaissance LA-ICP-MS to obtain semi-quantitative results for the REE together with bulk major and trace element analysis, grain size distributions, and TEM investigation of samples collected from mechanical and ESP hoppers. However, the available LA-ICP-MS spot size (100 μm) was too large to analyze REE-bearing domains found within these samples by SEM and TEM, and the matrix of NIST standard glasses used for standardization differed from that of measured particles. Thompson et al. (2016, 2018) emphasized ablation of fine-grained (less than 2 μm) REE-bearing trace phases such as zircon, apatite, and monazite found to be embedded in aluminosilicate glasses in two U.S. fly ash samples; the presence of REE trace phases was revealed both in LA-ICP-MS depth profiles and corresponding SEM-EDS studies. LA-ICP-MS quantification for 36 elements, including REE, in randomly selected spots was achieved by internal summation of results to 100%, rather than by use of external standards, with excellent results for all 36 elements determined in NIST SRM 610 run as an unknown (Thompson et al., 2018).

2.3.2 SHRIMP-RG ion microprobe

Compared to smaller SIMS instruments, and especially LA-ICP-MS, deployment of sensitive high-resolution ion microprobe (SHRIMP) facilities is much more limited. These large format instruments were developed in the late 1970s at Australian National University in order to

conduct grain-scale isotopic studies of geologic materials (Ireland et al., 2008). The primary application of this instrumentation is for radiometric dating using U-Th-Pb isotopes. A later generation of the SHRIMP with reversed geometry (SHRIMP-RG) allowed ultra-high mass resolution, especially useful in isotopic studies, and providing superior resolution of isobaric interferences in trace element determinations. Using electron beam methods and the Stanford/USGS SHRIMP-RG ion microprobe (Bacon et al., 2012), Kolker et al. (2017) studied a suite of fly ash samples from eastern, Illinois Basin, and western U.S. coals and determined REE contents of ash constituents on a grain scale. .. These authors were especially interested in determining the distribution of lanthanide REE in fly ash glasses, following from Hower et al. (2013a), who obtained counts for Ce in such glasses, but were limited by detection limits of the electron beam instrumentation. Results from the SHRIMP-RG show that glasses consisting almost entirely of Al and Si (aluminosilicates) had REE distributions comparable to or slightly below the bulk fly ash, whereas aluminosilicate glasses that also contained Fe or Ca trended towards higher REE contents (Figure 7). SHRIMP-RG analysis of co-occurring Fe-oxides showed that these also contain REE, confirming, on a grain scale, the findings of Yang et al (2014) for Fe-oxides separated from fly ash. As might be predicted from its crystal chemistry, quartz present in fly ash contains little or no REE and is essentially a diluent in efforts to recover REE from fly ash.

2.4 Synchrotron-based techniques

Another strategy to discern the chemical form of individual rare earth elements in coal fly ash is to employ synchrotron X-ray spectroscopy-based techniques. For those REE of relatively high abundance in fly ash samples (such as La, Ce, Nd, and Y), X-ray absorption spectroscopy of a fly ash sample allows the assessment of bulk-level element speciation. For example, bulk

XANES has been used to identify major phases of Ce, Nd, and Y, primarily through linear combination fitting models of the sample spectrum with spectra of reference compounds (Stuckman et al., 2018; Taggart et al., 2018b; Liu et al., 2019). The analyses generate relative percentages of the element as different reference species. This approach generally requires careful selection of known reference materials that could be reasonable approximations of the elemental forms in fly ash. Thus, the selection of reference materials must consider the conditions of fly ash formation and collection. This selection process can be especially challenging if the individual elements distribute diffusely within aluminosilicate glasses. In this case, the commercially available materials do not readily represent the localized coordination states of REE, nor are they easy to mimic in laboratory-synthesized materials.

The utility of XANES analyses is often limited by the relatively high concentration requirements of the method, particularly as coal-combustion fly ash is also enriched in other elements that might be interfering (Table1). Quantitative identification of species also requires sufficient differences in the spectral features of candidate reference compounds, which can be difficult to achieve *a priori*. In a previous application of yttrium K-edge XANES for coal fly ash (Taggart et al., 2018b), the spectral features of a yttrium carbonate mineral ($Y_2(CO_3)_3 \cdot 3H_2O$) were very similar to Y-doped glass and monazite reference materials. Thus, in the fitting of XANES spectra for coal fly ash samples, the replacement of one of these references with the other did not substantially alter the quality of the model fits. These subtleties emphasize the need for careful and cautious interpretation of XANES results. In other words, often the results are limited to qualitative descriptions (e.g. Samples A and B are similar or different in Y speciation), rather than quantitative interpretations (e.g., the 20% $Y_2(CO_3)_3$ in sample A is significantly different from 25% $Y_2(CO_3)_3$ in Sample B).

For elements that can exist in multiple oxidation states (e.g., Ce), bulk XANES can be especially useful for quantitative analysis of chemical form. For example, a recent study by Stuckman *et al.* (2018) demonstrated that greater than 85% of the Ce is in the Ce(III) form, suggesting that Ce is mostly distributed within the glassy matrix of fly ash and less frequently as distinct Ce minerals (e.g., CeO_2). The predominance of Ce(III) over Ce(IV) forms also supports the use of Ce as a proxy for other rare earth elements that share the trivalent ionic form.

The analysis of extended X-ray absorption fine structure (EXAFS) data can be used to determine the local bonding environment of the absorber atom (generally up to 5 Å). Insights provided by EXAFS techniques such as coordination number and bond distance can further help differentiate compounds (i.e., between Y-O and Y-P structures) and complement results of the XANES analysis. However, in the recent studies that employed bulk X-ray absorption spectroscopy for Ce and Y (Stuckman et al., 2018; Taggart et al., 2018b; Liu et al., 2019), the samples were not sufficiently concentrated to allow for EXAFS analysis. Thus, more work with EXAFS or other similar bulk elemental speciation methods is need to improve the quantitative determination of REE chemical forms in fly ash.

X-ray microprobe configurations at synchrotron beamlines enable similar analyses at 1-10 μm spatial resolution, and more recent advances have improved this resolution to the nanometer scale (Ice et al., 2011). Spatially resolved approaches allow for "mapping" of element composition (via microprobe X-ray fluorescence spectroscopy (μXRF)). Element maps via μXRF require careful interpretation due to overlapping signals of multiple elements (i.e., non-unique assignments are possible). For example, V and Ba emission signals were previously observed to overlap with Ce emission energies (Stuckman et al., 2018). Regardless, for spots of sufficient concentration, micro-XANES and micro-EXAFS can discern the chemical form of the

target element. For REE in coal fly ash, this approach can help identify 'hotspots' – i.e., discrete particles of REE-bearing minerals associated with or encapsulated in the ash matrix. While developments at microprobe beamlines represent a forefront of synchrotron-based techniques, their application for understanding REE recovery potential from fly ash is somewhat limiting because these hotspots represent a small proportion of the total element in fly ash particles.

2.5 Electron Microscopy

Electron microscopic examination of fly ash and bottom ash generally begins with SEM and energy-dispersive X-ray spectroscopy (EDX) examination of either powder samples or epoxy-mounted and polished pellets (as were used for optical petrography) (for example Hood et al., 2017; Hower et al. 2017b, 2018a, 2019). Individual minerals or mineral assemblages of interest are isolated and extracted by a dual-beam Focused Ion Beam (FIB)/SEM in order to monitor the chemistry of the minerals during the extraction process. Following FIB extraction, samples are thinned to less than 100 μm for examination by transmission electron microscopy (TEM) and related techniques. Selected area electron diffraction (SAED) is employed for mineralogical identification of grains. Either in conjunction with SAED or for grains too small for SAED, mineral identification can be accomplished with high resolution TEM (HRTEM). Fast Fourier transform (FFT), computed by image analysis software, is used to determine the lattice spacing in HRTEM micrographs. Chemical identification in TEM is available in some units via electron energy loss spectroscopy (EELS).

REE-bearing minerals observed by TEM in select eastern Kentucky coals include a mixed monazite/kaolinite grain from the Fire Clay coal (Figure 8) (Hower et al., 2018b, 2018c). The Fire Clay coal is of particular interest as a REE resource as the coal, as the coal preparation products (Honaker et al., 2018; Zhang and Honaker, 2018; Zhang et al., 2018; Huang et al.,

2018), and as the fly ash resulting from the coal utilization (Zhang et al., 2015; Hower et al., 2015, 2017b, 2020b; Hood et al., 2017). In the case illustrated here, the original layered monazite and volcanic glass from the volcanic ash fall (Hower et al., 2016b) were altered to a monazite/kaolinite mixed grain. The Manchester coal, Clay County, eastern Kentucky, contains florencite ($(REE)Al_3(PO_4)_2(OH)_6$) nodules (Hower et al., 2020a).

As shown by optical petrology (section 2.2), monazite and other REE-bearing minerals occur in combustion ashes. Figure 9 illustrates a relatively large La-Ce-Nd monazite grain with a Y-rich xenotime inclusion. Small (tens of nm) REE-phosphate grains on a mullite crystal are shown on Figure 10. Mullite is a more important constituent of this ash as compared to most fly ashes due to the larger particle size and the consequent longer cooling time of the stoker ash; the mineral has the time required to crystallize versus the formation of an Al-Si glass (also see Figure 5 for an optical view of the same ash). In contrast to the visible minerals in the latter ashes, other REE-rich areas have no discernable minerals (Figure 11). In this case, while there is an indication (via SAED) of crystallinity, the minerals are too small, overlap, and/or have disparate orientations, making mineral identification impossible with current techniques. In addition to monazite and Y-bearing zircon, davidite-Ce ($(Ce,La)(Y,U)(Ti,Fe)_{20}O_{38}$) or $(Ce,La)(Y,U, Fe)(Ti,Fe)_{20}(OH,O)_{38}$)) was found in a stoker ash from the combustion of the Fire Clay coal (Hower et al., 2019).

Studies of fly ash carbons (Hower et al., 2008, 2017a, b; Wilcox et al., 2015; Hood et al., 2017; Hower and Groppo, 2020) indicate that graphitic and fullerene-like carbons, often with included/entrained few-nm minerals and/or metals, occur in the fly ash resulting from the combustion of bituminous coals. Spinel minerals (Figure 12 and 13) occur in association with REE; for example, Ce found within the carbon surrounding the Fe-spinel (Figure 12C).

Similarly, Nd, Ce, Sm, and Y occur in the carbon surrounding a spinel from the same fly ash (Figure 13). Figure 14 illustrates an Al-Si glass with an Fe-O core, possibly spinels, surrounded by Ce-Nd-Sm-Y-graphitic carbon. Another grain showing the dispersion of the Nd and Ce in the carbon surrounding the Al-Si glass is shown on Figure 15. The EDX carbon overlapping the Al-Si glass is blacked out on the upper right image, concealing the dense Nd and Ce concentrations coincident with the glass. The TEM image and the derivative EDX scans are really capturing some semblance of three dimensions; therefore, the REE elements overlying the glass appear to be associated with the carbon, just as they are in the carbon corona adjacent to the glass. EELS imaging of a fly ash particle shows Ce to be associated with needle-shaped minerals (Figure 16), an occurrence similar to that in Figure 10, above.

3. EXTRACTIONS AND SEPARATIONS FOR REE RECOVERY FROM FLY ASH

The extraction of REEs and other critical metals from fly ash and bottom ash requires a combination of acid leaching (or roasting followed by acid leaching), physical separations, and ion separation processes (Zhang et al., 2020; Rybak and Rybak, 2021). Economically feasible methods to produce saleable REE products from coal fly ash have yet to be fully proven and research on methods remain in early stages of development.. In the development of REE extraction methods, lessons can be learned from past studies on recovery of other elements (e.g., aluminum and germanium) from fly ash and from the processes used to recover REEs at conventional mining operations (Arroyo and Fernández-Pereira, 2008; Bai et al., 2011; Fang and Gesser, 1996; Gilliam et al., 1982; Kelmers et al., 1982; Meawad et al., 2010; Molycorp Minerals LLC, 2010; Dai et al., 2014b, 2014c; Rayzman et al., 1997).

At traditional mining sites, ores are first excavated and then processed to finer particles using milling, crushing, and grinding units (Molycorp Minerals LLC, 2010; Peak Resources

Limited, 2017) (Figure 17). As this step would not be necessary for coal ash, the first step involves physical separations such as sieving, magnetic separation, or froth flotation to remove materials with low-REE content and/or materials which would interfere with the downstream processing (e.g., high Fe-content and/or high-C-content particles). For example, slight enrichment of REE contents have been observed in the non-magnetic fraction and small size fraction (<200 mesh) of coal fly ashes (Blissett et al., 2014; Lin et al., 2017b). Thus, preprocessing steps to remove magnetic and coarse material aid in the concentration of REE as well as remove interferences (such as iron) for downstream ion separations.

Physical separations are followed by a leaching step that typically requires strong acids (e.g., sulfuric, nitric, or hydrochloric acids) to solubilize the metals from the material. For a subset of coal fly ashes, such as Ca-rich fly ashes that are characteristic of western U.S. coals, acid leaching is usually sufficient for full extraction of REE (Cao et al., 2018; King et al., 2018). For other coal fly ashes, an alternative process could entail alkaline treatment that decomposes aluminosilicate glasses (Bai et al., 2010; McDowell and Seeley, 1981; Padilla and Sohn, 1985; Querol et al., 2002). This approach might be implemented as a wet alkaline digestion or a dry roasting process as a way to convert the REEs in coal fly ash to an acid-soluble phase (Honaker et al., 2019; King et al., 2018; Lin et al., 2018b; Taggart et al., 2018a; Wang et al., 2019; Yakaboylu et al., 2019).

After the extraction of REE from the fly ash, the REEs need to be further purified from the aqueous acidic mixture. In conventional REE hydrometallurgical processes, this step often entails liquid-liquid separations, selective precipitation, or solid phase extraction (Hu et al., 2018). For leachates of coal-derived fly ash and other geologically-derived brine solutions, researchers have proposed a wide variety of approaches to purify REEs. In one patented method

(Joshi et al., 2013), researchers proposed a combination of an organophosphate chelating compound (e.g., tributylphosphate) saturated in an organic phase (e.g., kerosene) to selectively separate the trivalent rare earth cations over other ions, followed by back extraction into the aqueous phase and recycling of the organic solvent. This liquid-liquid (solvent) extraction approach closely mimics methods utilized for traditional recovery of uranium and REEs from ores (Brown and Sherrington, 1979; Flett, 2005). Other methods for purification could also include selective precipitation of Fe- and Al-hydroxides through the addition of sodium hydroxide or lime (Mutlu et al., 2018; Middleton et al., 2020), and while these approaches are favorable from a scalability perspective, they tend to have relatively high operating expenses due to substantial requirements for reagents to adjustment pH.

Several other ion separation methods have been proposed for the separation of coal fly ash and other geological waste materials, including ion exchange, sorption, and membrane filtration (Callura et al., 2018; Das and Das, 2013; Kose-Mutlu et al., 2020; Lo et al., 2014; Mutlu et al., 2018; Park et al., 2017; Park et al., 2020; Smith et al., 2019). Other REE purification technologies that have been directly tested on fly ash leachates include biosorption with bacterial cells that have been genetically engineered to express lanthanide binding tags on their cell envelope (Park et al., 2017; Park et al., 2020). Others have attempted supported liquid membranes (Smith et al., 2019), a liquid-liquid extraction approach that entails the use of a hydrophobic membrane embedded with an organic solvent/extractant mixture. Likewise, nanomaterial-enabled electrochemical methods for REE separation and recovery have the potential to selectively precipitate REEs due to local generation of hydroxide (from water and oxygen) that serves to precipitate mixed rare earth oxide and hydroxide cakes (O'Connor et al., 2018). Other novel, nano-enabled sorbents or chelating agents that have the potential to separate

REEs selectively are being explored but have not yet been assayed against the complex mixture of coal ash (Rahman et al., 2020; Bie et al., 2020; Hamza et al., 2021; Chen et al., 2020). While filtration-based methods could provide advantages relative to conventional solvent extraction methods by reducing liquid chemical consumption, decreasing the footprint of the process and enhancing modularity, the primary barriers towards applying these technologies for coal ash are the relatively low purity REE content and the high abundance of interfering ions (e.g., Si, Al, Fe) that co-leach with the REE during processing (see Figure 18). Nevertheless, selective pre-treatments or future innovations may help surmount those challenges.

4. OUTLOOK AND RESEARCH NEEDS

The realization that coal fly ash can be a large and untapped reserve for REEs has sparked great interest for recovery technologies, particularly with motivations to increase the diversity of the global REE supply market. Furthermore, additional reuse markets for coal fly ash could decrease disposal needs for coal ash, the largest industrial waste streams for nations heavily reliant on coal energy. As noted previously, existing hydrometallurgical methods for REE separations are now in early stages of development. However, scale-up of these processes for profitable recovery of REE products remains elusive. Ongoing challenges in the recovery and concentration of REE from fly ash could offer another benefit – innovations in separation technologies (such as those described in later chapters of this volume) that could greatly advance the overall field of metals separation and waste reuse.

Major challenges currently hinder successful and sustainable recovery of REE from coal fly ash. First, the enrichment of REEs in coal fly ash is *low* relative to REE contents of ores found at rare earth mines or REE contents in other secondary feedstocks (e.g., electronic wastes, where there has been much development in extraction efforts; e.g., Bahaloo-Horen et al., 2020;

Makarova et al., 2020). As such, recovery operations must overcome high hurdles in extraction and separation efficiency. Potential processes must be especially selective for rare earth metal ions because other major elements such as Na, K, Ca, Mg, Fe, Al, and Si are 10^4 to 10^6 times more concentrated than individual rare earths in fly ash leachates (King et al., 2018: Taggart et al., 2018a). Metal ions of Fe, Ca, and Al could be especially problematic given their high abundance as well as moderate to high affinity for ion exchange resins and chelating agents used to purify REEs (King et al., 2018: Taggart et al., 2018a). Elements of health concern, such as uranium (U) and thorium (Th), also require strategic separation and present a technological challenge that has long been identified but remains in nascent stages of investigation (Bie et al., 2020). Thus, pre-processing steps may be essential to reduce these interfering ions (and pH adjustments with NaOH, which adds interfering ions, may be counterproductive). Moreover, the challenge of moderate levels of enrichment requires novel separations that improve REE selectivity as a means to recover REE materials of saleable purity.

Second, development of an environmentally sustainable REE recovery process is a major challenge in REE separations from fly ash. With previous work demonstrating that complete dissolution of fly ash particles may be required to fully liberate REEs into solution (Hower et al., 2017b), large volumes of chemicals including strong acids and organic solvents may be required for REE recovery operations. New innovations in process engineering are needed to facilitate recycling these chemicals during the recovery process, both to keep operating expenses low and to avoid the generation of another large-volume waste stream. Moreover, novel REE separation approaches could aim to reduce the usage of chemicals, especially organic solvents. Advanced sorbents, ion exchange resins, electrochemical or biosorption methods, or new configurations of liquid-liquid separations might offer benefits in this respect (Callura et al., 2018; Kim et al.,

2015; Park et al., 2020; O'Connor et al., 2018; Smith et al. 2019; Couto et al., 2020), as long as they can overcome needs for REE selectivity.

Finally, with REE recovery technologies from fly ash still in their infancy, current techno-economic analyses are fraught with high degrees of uncertainty. Chemical consumption and waste handling are likely to be major contributors to costs (Das et al., 2018; Hendren et al., 2017) and therefore, these need careful consideration as innovations progress. As noted previously, revenue estimates in these assessments are highly reliant upon the value of Sc in fly ash. Of the REE elements, Sc is currently one of the highest valued on a price per kg basis, but it is also produced at low volumes. For example, on 28 February 2020, Sc was priced at $U.S. 3487 per kg (Berlet and Samnani, 2020) and global production was 15-20 tons (Gambogi, 2017). In contrast, the market price on the element basis of Ce and Nd, with 24,000 and 33,000 tons of global production, respectively, is $U.S. 4.59 per kg and $US 52.66 per kg, respectively (28 February 2020 from Berlet and Samnani, 2020; based on 22 June 2020 Chinese Yuan to US Dollar conversion). The recovery of Sc from coal fly ash may inundate the Sc supply market, resulting in a decrease in the market price for this commodity and much lower revenue potential than values in current estimates. These uncertainties suggest that the design of REE recovery technologies would greatly benefit by other saleable products generated in the process. Thus, engineering for co-production is likely to be essential for overcoming these challenges and the attainment of REE production from coal combustion residuals.

Acknowledgments. Portions of this study were completed as part of U.S. Department of Energy contracts DE-FE0027167 and DE-FE0026952 and were further supported by National Science Foundation grants CBET-1510965 and CBET-1510861 to Duke University and the University of Kentucky, respectively. Hower's work was further supported by U.S. Department of Energy contract DE-FE0029007 to the University of North Dakota Energy & Environmental Research Center with a subcontract to the University of Kentucky.

This work used shared facilities at the Virginia Tech National Center for Earth and Environmental Nanotechnology Infrastructure (NanoEarth), a member of the National Nanotechnology Coordinated Infrastructure (NNCI), supported by NSF (ECCS 1542100). Michael Hochella, Jr., Christopher Winkler, Debora Berti, Elizabeth Cantando, and Mitsu Murayama assisted us at Virginia Tech.

Access to characterization instruments and staff assistance at the University of Kentucky was provided by the Electron Microscopy Center, supported in part by the National Science Foundation/EPSCoR Award No. 1355438 and by the Commonwealth of Kentucky. Uschi Graham, Madison Hood, Dali Qian, Nicolas Briot, Jason Unrine, Jack Groppo, Tristana Duvallet, and Bob Jewell assisted at the University of Kentucky.

Clint Scott and Jorge Vazquez (USGS), and Matt Coble (Stanford University) are acknowledged for their help in acquiring SHRIMP-RG data. Use of the SHRIMP-RG was supported by a Technical Assistance Agreement between the USGS and the University of Kentucky, with funding from U.S. Department of Energy contract DE-FE0027167, and from the USGS Energy Resources Program. Any use of trade, firm, or product names is for descriptive purposes and does not imply endorsement by the U.S. Government.

REFERENCES

Alekseev, Yu.I., Vereshchagin, V.I. (1997). Formation of crystalline phases in electroceramics of the system $CaO-MgO-Al_2O_3-SiO_2$ (A review). *Glass and Ceramics, 54*, 340-343.

American Coal Ash Association (2019). Coal ash recycling rate declines amid shifting production and use patterns. https://www.acaa-usa.org/publications/productionusereports.aspx. (accessed 17 June 2020)

Arroyo, F., Fernández-Pereira, C. (2008) Hydrometallurgical recovery of germanium from coal gasification fly ash. Solvent extraction method. *Industrial & Engineering Chemistry Research, 47*, 3186-3191.

ASTM International (2017). ASTM C618-17, Standard specification for coal fly ash and raw or calcined natural pozzolan for use in concrete: ASTM International website, https://www.astm.org/Standards/C618.htm.

Bacon, C.R., Grove, M., Vazquez, J.A., Coble, M.A. (2012). The Stanford-U.S. Geological Survey SHRIMP ion microprobe- A tool for micro-scale chemical and isotopic analysis. *U.S. Geological Survey Fact Sheet 2012-3067*, 4 p.

Bahaloo-Horeh, N., Mousavi, S.M. (2020). Comprehensive characterization and environmental risk assessment of end-of-life automotive catalytic converters to arrange a sustainable roadmap for future recycling practices. *Journal of Hazardous Materials, 400*, 123186.

Bai, G.-h., Teng, W., Wang, X.-g., Qin, J.-g., Xu, P., Li, P.-c. (2010). Alkali desilicated coal fly ash as substitute of bauxite in lime-soda sintering process for aluminum production. *Transactions of Nonferrous Metals Society of China, 20*, 169-175.

Bai, G., Qiao, Y., Shen, B., Chen, S. (2011). Thermal decomposition of coal fly ash by concentrated sulfuric acid and alumina extraction process based on it. *Fuel Processing Technology, 92*, 1213-1219.

Balashov, Y.A. (1976). *Geochemistry of Rare Earth elements*. Nauka, Moscow, 267 p. (in Russian)

Bank, T.L., Roth, E.A., Tinker, P., Granite, E., (2016). Analysis of Rare Earth Elements in Geologic Samples using Inductively Coupled Plasma Mass Spectrometry. U.S. DOE Topical Report - DOE/NETL-2016/1794.

Basu, Z., (2017). In the heart of coal country, state officials bet on renewable energy. *CNBC*, 18 July 2017, http://www.cnbc.com/2017/07/18/post-coal-country-kentucky-bets-on-renewable-energy-metals-mining.html, accessed 17 June 2020.

Bauer, G., Achleitner, B., Bonta, M., Friedbacher, G., Limbeck, A. (2017). Analysis of single fly ash particles using laser ablation ICP-MS-an approach achieving lateral elemental distribution information via imaging. *RSC Advances, 7(33),* 20510-20519. doi:10.1039/C7RA00975E

Berlet, C.J., Samnani, K. (2020) Mineral Prices.com. https://mineralprices.com/rare-earth-metals/ (accessed 22 June 2020)

Bie, C., Gao, Y., Su, J., Dong, Y.M., Guo, X.G., Sun, X.Q. (2020). The efficient separation of thorium from rare earth using oxamic acid in hydrochloric acid medium. *Separation and Purification Technology, 251,* 117358.

Blissett, R. S., Smalley, N., & Rowson, N. A. (2014). An investigation into six coal fly ashes from the United Kingdom and Poland to evaluate rare earth element content. *Fuel, 119*, 236-239.

Bragg, L.J., Oman, J.K., Tewalt, S.J., Oman, C.L., Rega, N.H., Washington, P.M., Finkelman, R.B. (1998). *U.S. Geological Survey Coal Quality (COALQUAL) database: Version 2.0*. U.S. Geological Survey Open-file Report 97-134, CD-ROM.

Brown, C.G., Sherrington, L.G. (1979) Solvent extraction used in industrial separation of rare earths. *Journal of Chemical Technology and Biotechnology,* 29, 193-209.

Brownfield, M.E., Affotter, R.H., Brownfield, I.K., Hower, J.C., Stricker, G.D. (1999). *Dispersed volcanic ash in feed coal and its influence on coal combustion products*. International Ash Utilization Symposium, Lexington, KY, 18-20 October 1999, paper #61, http://www.flyash.info (Accessed 22 June 2020)

Brownfield, M.E., Cathcart, J.D., Affolter, R.H., Brownfield, I.K., Rice, C.A., O'Connor, J.T., Zielinski, R.A., Bullock, J.H., Jr., Hower, J.C., Meeker, G.P., (2005). *Characterization and modes of occurrence of elements in feed coal and coal combustion products from a power plant utilizing low-sulfur coal from the Powder River Basin, Wyoming*. U.S. Geological Survey Scientific Investigations Report 2004-5271, 36 p., https://pubs.usgs.gov/sir/2004/5271/.

Callura, J.C., Perkins, K.M., Noack, C.W., Washburn, N.R., Dzombak, D.A., Karamalidis, A.K. (2018) Selective adsorption of rare earth elements onto functionalized silica particles. *Green Chemistry, 20*, 1515-1526.

Cao, S., Zhou, C., Pan, J., Liu, C., Tang, M., Ji, W., Hu, T., Zhang, N. (2018) Study on Influence Factors of Leaching of Rare Earth Elements from Coal Fly Ash. *Energy & Fuels, 32*, 8000-8005.

Chen, Z.L., Yang, X.Y., Song, L.J., Wang, X.Y., Xiao, Q,, Xu, H.W., Feng, Q.X., Ding, S.D. (2020). Extraction and complexation of trivalent rare earth elements with tetraalkyl diglycolamides. *Inorganica Chimica Acta, 513*, 119928.

Chenery, S., Querol, X., and Fernández-Turiel, J.L. (1995) Quantitative determination of trace element affinities in coal and combustion wastes by Laser Ablation Microprobe- Inductively Coupled Plasma – Mass Spectrometry: in, Pajares, J.A., and Tascón, eds., *Coal Science, Proceedings of the Eighth International Conference on Coal Science*, Elsevier, p. 327-330.

Cherniak, D.J., Watson, E.B. (2013). Diffusion of helium in natural monazite, and preliminary results on He diffusion in synthetic light rare earth phosphates. *American Mineralogist, 98*, 1407-1420.

Cherniak, D.J., Watson, E.B., Thomas, J.B. (2009). Diffusion of helium in zircon and apatite. *Chemical Geology, 268*, 155-166.

Clarke, L.B., Sloss, L.L. (1992). Trace elements- emissions from coal combustion and gasification. *IEA Coal Research, IEACR/49*, 111 p.

Connelly, N. G., Hartshorn, R. M., Damhus, T., & Hutton, A. T. (Eds.). (2005). *Nomenclature of inorganic chemistry: IUPAC recommendations 2005*. Royal Society of Chemistry.

Couto, N., Ferreira, A.R., Lopes, V., Peters, S.C., Mateus, E.P., Ribeiro, A.B., Pamukcu, S. (2020). Electrodialytic recovery of rare earth elements from coal ashes. *Electrochimica Acta, 359,* 136934.

Dai, S., Luo, Y., Seredin, V.V., Ward, C.R., Hower, J.C., Zhao, L., Liu, S., Tian, H., Zou, J. (2014a). Revisiting the late Permian coal from the Huayingshan, Sichuan, southwestern China: Enrichment and occurrence modes of minerals and trace elements. *International Journal of Coal Geology, 122*, 110–128.

Dai, S., Seredin, V.V., Ward, C.R., Jian, J., Hower, J.C., Song, X., Jiang, Y., Wang, X., Gornostaeva, T., Liu. H., Zhao, L. (2014b). Composition and modes of occurrence of minerals and elements in coal combustion products derived from high-Ge coals. *International Journal of Coal Geology*, 121, 79-97.

Dai, S., Zhao, L., Hower, J.C., Johnston, M.N., Song, W., Wang, P., Zhang, S. (2014c). Petrology, mineralogy, and chemistry of size-fractioned fly ash from the Jungar power plant, Inner Mongolia, China, with emphasis on the distribution of rare earth elements. *Energy & Fuels*, 28, 1502–1514.

Dai, S., Graham, I.T., Ward, C.R. (2016a). A review of anomalous rare earth elements and yttrium in coal. *International Journal of Coal Geology, 159*, 82-95.

Dai, S., Liu, J., Ward, C.R., Hower, J.C., French, D., Jia, S., Hood, M.M., Garrison, T.M. (2016b). Mineralogical and geochemical compositions of Late Permian coals and host rocks from the Guxu Coalfield, Sichuan Province, China, with emphasis on enrichment of rare metals. *International Journal of Coal Geology, 166*, 71-95.

Dai, S., Xie, P., Jia, S., Ward, C.R., Hower, J.C., Yan, X., French, D. (2017). Enrichment of U-Re-V-Cr-Se and rare earth elements in the Late Permian coals of the Moxinpo Coalfield, Chongqing, China: Genetic implications from geochemical and mineralogical data. *Ore Geology Reviews, 80*, 1–17.

Das, N., Das, D. (2013) Recovery of rare earth metals through biosorption: An overview. *Journal of Rare Earths, 31*, 933-943.

Das, S., Gaustad, G., Sekar, A., Williams, E. (2018). Techno-economic analysis of supercritical extraction of rare earth elements from coal ash. *Journal of Cleaner Production, 189*, 539-551.

Dobransky, S. (2013). Rare Earth Elements and U.S. Foreign Policy: The Critical Ascension of REEs in Global Politics and U.S. National Security. *American Diplomacy,* http://www.unc.edu/depts/diplomat/item/2013/0912/ca/dobransky_rareearth.html

Ehlers, E.G. (1972). *The interpretation of geological phase diagrams*. San Francisco, W.H. Freeman & Co., 280 p.

Energy Information Administration (2017). *Electricity*. https://www.eia.gov/electricity/monthly/update/archive/july2017/ (Accessed 22 June 2020).

Energy Information Administration (2020). *Coal*. https://www.eia.gov/coal/ (accessed 17 June 2020).

Energy Information Administration. (2018). *U.S. electricity data*. https://www.eia.gov/electricity/data.php, (Accessed 22 June 2020).

Environmental Protection Agency (2019). *Final Cross-State Air Pollution Rule Update.*. http://www.epa.gov/ airmarkets/final-cross-state-air-pollution-rule-update (Accessed 22 June 2020).

Environmental Protection Agency (2020). *Regulatory Actions - Final Mercury and Air Toxics Standards (MATS) for Power Plants.* https://www.epa.gov/mats/regulatory-actions-final-mercury-and-air-toxics-standards-mats-power-plants (Accessed 22 June 2020).

Environmental Protection Agency [EPA]. (2014). *Final Rule—Disposal of coal combustion residuals from electric utilities.* https://www.epa.gov/coalash/coal-ash-rule. (Accessed 22 June 2020)

Eskanazy, G.M. (1987a). Rare earth elements in a sampled coal from the Pirin deposit, Bulgaria. *International Journal of Coal Geology, 7*, 301-314.

Eskanazy, G.M. (1987b). Rare earth elements and yttrium in lithotypes of Bulgarian coal. *Organic Geochemistry, 11*, 83-89.

Eskanazy, G.M. (1999). Aspects of the geochemistry of rare earth elements in coal: An experimental approach. *International Journal of Coal Geology, 38*, 285-295.

Fang, Z., Gesser, H. (1996) Recovery of gallium from coal fly ash. *Hydrometallurgy, 41*, 187-200.

Farley, K.A. (2007). He diffusion systematics in minerals: Evidence from synthetic monazite and zircon structure phosphates. *Geochimica et Cosmochimica Acta, 71*, 4015-4024.

Finch, R.J., Hanchar, J.M. (2003). Structure and chemistry of zircon and zircon group minerals, in Hanchar, J.M., and Hoskin, P.W.O., eds., Zircon. *Mineralogical Society of America, Reviews in Mineralogy and Geochemistry, 53*, 1-25.

Finkelman, R.B. (1981). Modes of occurrence of trace elements in coal. *U.S. Geological Survey Open File Report 81-99*, 301 p.

Finkelman, R.B. (1993). Trace and minor elements in coal, in Engel, M.H., and Macko, S.A., eds, *Organic Geochemistry, Principles and Applications*: New York, Plenum Press, p. 593–607, https://doi.org/10.1007/978-1-4615-2890-6_28.

Flett, D.S. (2005) Solvent extraction in hydrometallurgy: the role of organophosphorus extractants. *Journal of Organometallic Chemistry, 690*, 2426-2438.

Fortier, S.M., Nassar, N.T., Lederer, G.W., Brainard, J., Gambogi, J., McCullough, E.A., (2018). Draft critical mineral list—Summary of methodology and background information—U.S. Geological Survey technical input document in response to Secretarial Order No. 3359: U.S. Geological Survey Open-File Report 2018–1021, 15 p., https://doi.org/10.3133/ofr20181021.

Gambogi, J. (2020) Mineral commodity summaries, January 2020. U.S. Geological Survey. https://minerals.usgs.gov/minerals/pubs/commodity/scandium/mcs-2020-scand.pdf (accessed 22 June 2020)

Gilliam, T., Canon, R., Egan, B., Kelmers, A., Seeley, F., Watson, J. (1982). Economic metal recovery from fly ash. *Resources and Conservation, 9*, 155-168.

Goldschmidt, V.M. (1935). Rare elements in coal ashes: *Industrial and Engineering Chemistry, 27*, 1100–1102, https://doi.org/10.1021/ie50309a032.

Greene, J. (2012). *Digging for rare earths: The mine where iPhones are born*. http://www.cnet.com/news/digging-for-rare-earths-the-mines-where-iphones-are-born/ (Accessed 22 June 2020)

Gromet, L.P., Dymek, R.F., Haskin, L.A., and Korotev, R.L. (1984), The "North American shale composite": Its compilation, major and trace element characteristics: *Geochimica et Cosmochimica Acta, v. 48*, p. 2469-2482.

Guenthner, W.R., Reiners, P.W., Ketcham, R.A., Nasdala, L., Giester, G. (2013). Helium diffusion in natural zircon: radiation damage, anisotropy, and the interpretation of zircon (U-Th)/He thermochronology. *American Journal of Science, 313*, 145-198.

Hamza, M.F., Salih, K.A.M., Abdel-Rahman, A.A.H., Zayed, Y.E., Wei, Y.Z., Liang, J., Guibal, E. (2021). Sulfonic-functionalized algal/PEI beads for scandium, cerium and holmium sorption from aqueous solutions (synthetic and industrial samples). *Chemical Engineering Journal, 403*, 126399.

Hanson, G.N. (1980). Rare earth elements in petrogenetic studies of igneous systems. *Annual Reviews of Earth and Planetary Sciences, 8*, 371-406.

Harkins, W. D. (1917). "The Evolution of the Elements and the Stability of Complex Atoms". *Journal of the American Chemical Society, 39*,856. doi:10.1021/ja02250a002.

Hatch, G.P. (2012). Dynamics in the Global Market for Rare Earths. *Elements* 8, 341-346.

Hendren, A., Choi, Y.C., Hsu-Kim, H., Hower, J.C., Plata, D., Wiesner, M. (2017). Preliminary techno-economic evaluation of a novel membrane based separation and recovery process for rare earth elements from coal combustion residues. World of Coal Ash Proceedings, 9-11 May 2017, Lexington, KY, paper 149, http://www.flyash.info/AshSymposium/AshLibraryAuthors.asp#H (Accessed 22 June 2020)

Hikichi, Y., Nomura, T. (1987). Melting temperatures of monazite and xenotime. *Journal of the American Ceramic Society, 70*, C252-C253.

Hoff, S. (2017). *Competition between coal and natural gas affects power markets*. U.S. Energy Information Administration, 16 June 2017, https://www.eia.gov/todayinenergy/detail.php?id=31672 (Accessed 22 June 2020).

Home, A. (2020). U.S. finds its Chinese rare earth dependency hard to break. *Reuters*, https://uk.reuters.com/article/us-usa-rareearths-ahome/column-u-s-finds-its-chinese-rare-earth-dependency-hard-to-break-idUKKCN24T20I (accessed 31 July 2020)

Honaker, R.Q., Zhang, W., Yang, X., Rezaee, M. (2018). Conception of an integrated flowsheet for rare earth elements recovery from coal coarse refuse. *Minerals Engineering, 122*, 233-240. DOI: 10.1016/j.mineng.2018.04.005

Honaker, R. Q., Zhang, W., Werner, J. (2019). Acid Leaching of Rare Earth Elements from Coal and Coal Ash: Implications for Using Fluidized Bed Combustion To Assist in the Recovery of Critical Materials. *Energy & Fuels, 33*(7), 5971-5980.

Hood, M.M., Taggart, R.K., Smith, R.C., Hsu-Kim, H., Henke, K.R., Graham, U.M., Groppo, J.G., Unrine, J.M., Hower, J.C. (2017). Rare earth element distribution in fly ash derived from the Fire Clay coal, Kentucky. *Coal Combustion & Gasification Products, 9*, 22-33. doi:10.4177/CCGP-D-17-00002.1.

Houser, T., Bordoff, J., Marsters, P. (2017). *Can Coal Make a Comeback?* Columbia University School of International and Public Affairs, Center on Global Energy Policy, http://energypolicy.columbia.edu/publications/report/can-coal-make-comeback (accessed 22 June 2020).

Hower, J.C. (2012). Petrographic examination of coal-combustion fly ash. *International Journal of Coal Geology, 92*, 90-97.

Hower, J.C., Ruppert, L.F., Eble, C.F. (1999). Lanthanide, Yttrium, and Zirconium anomalies in the Fire Clay coal bed, Eastern Kentucky. *International Journal of Coal Geology,* 39, 141-153.

Hower, J.C., Graham, U.M., Dozier, A., Tseng, M.T., Khatri, R.A. (2008). Association of sites of heavy metals with nanoscale carbon in a Kentucky electrostatic precipitator fly ash. *Environmental Science & Technology, 42*, 8471-8477.

Hower, J.C., Groppo, J.G., Joshi, P., Dai, S., Moecher, D.P., Johnston, M.N. (2013a). Location of cerium in coal combustion fly ashes: Implications for recovery of lanthanides. *Coal Combustion and Gasification Products, 5*, 73-78, doi:10.4177/CCGP-D13-00007.1.

Hower, J.C., Dai, S., Seredin, V.V., Zhao, L., Kostova, I.J., Silva, L.F.O., Mardon, S.M., Gurdal, G. (2013b). A note on the occurrence of Yttrium and Rare Earth Elements in coal combustion products.

Coal Combustion and Gasification Products, 5, p. 39-47.

Hower, J.C., Groppo, J.G., Henke, K.R., Hood, M.M., Eble, C.F., Honaker, R.Q., Zhang, W., Qian, D. (2015). Notes on the potential for the concentration of rare earth elements and Yttrium in coal combustion fly ash. *Minerals, 5*, 356-366. doi:10.3390/min50x000x.

Hower, J.C., Granite, E.J., Mayfield, D., Lewis, A., Finkelman, R.B. (2016a). Notes on contributions to the science of rare earth element enrichment. *Minerals, 6*, doi:10.3390/min6020032.

Hower, J.C., Eble, C.F., Dai, S., Belkin, H.E. (2016b). Distribution of rare earth elements in eastern Kentucky coals: Indicators of multiple modes of enrichment? *International Journal of Coal Geology, 160-161*, 73-81. 10.1016/j.coal.2016.04.009

Hower, J.C., Groppo, J.G. (2020). Rare Earth-bearing particles in fly ash carbons: Examples from the combustion of eastern Kentucky coals. *Energy Geoscience*, https://doi.org/10.1016/j.engeos.2020.09.003

Hower, J.C., Groppo, J.G., Henke, K.R., Graham, U.M., Hood, M.M., Joshi, P., Preda, D.V. (2017b). Ponded and landfilled fly ash as a source of rare earth elements from a Kentucky power plant. *Coal Combustion & Gasification Products, 9*, 1-21. doi:10.4177/CCGP-D-17-00003.1.

Hower, J.C., Groppo, J.G., Graham, U.M., Ward, C.R., Kostova, I.J., Maroto-Valer, M.M., Dai, S. (2017a). Coal-derived unburned carbons in fly ash: A review. *International Journal of Coal Geology, 179*, 11-27. http://dx.doi.org/10.1016/j.coal.2017.05.007

Hower, J.C., Henke, K.R., Dai, S., Ward. C.R., French, D., Liu, S., Graham, U., 2017c. The generation and nature of coal fly ash and bottom ash. In: Robl, T.L., et al., *Coal Combustion Products*, Cambridge, MA, Woodhead Publishing (Elsevier), Chapter 2, p. 21-65. http://dx.doi.org/10.1016/B978-0-08-100945-1.00002-2.

Hower, J.C., Qian, D., Briot, N., Henke, K.R., Hood, M.M., Taggart, R.K., Hsu-Kim, H. (2018a). Rare earth element associations in the Kentucky State University stoker ash. *International Journal of Coal Geology, 189*, 75-82. 10.1016j.coal2018.02.022.

Hower, J.C., Berti, D., Hochella, M.F., Jr., Rimmer, S.M., Taulbee, D.N. (2018b). Submicron-scale mineralogy of lithotypes and the implications for trace element associations: Blue Gem coal, Knox County, Kentucky. *International Journal of Coal Geology, 192*, 73-82. https://doi.org/10.1016/j.coal.2018.04.006

Hower, J.C., Berti, D., Hochella, M.F., Jr., Mardon, S.M. (2018c). Rare Earth minerals in a "no tonstein" section of the Dean (Fire Clay) coal, Knox County, Kentucky. *International Journal of Coal Geology, 193*, 73-86. https://doi.org/10.1016/j.coal.2018.05.001.

Hower, J.C., Cantando, E., Eble, C.F., Copley, G.C., (2019). Characterization of stoker ash from the combustion of high-lanthanide coal at a Kentucky bourbon distillery. *International Journal of Coal Geology*, *213*, 103260. https://doi.org/10.1016/j.coal.2019.103260

Hower, J.C., Qian, D., Briot, N.J., Hood, M.M., Eble, C.F., (2020a). Nano-scale mineralogy of a Rare earth element-rich Manchester coal lithotype, Clay County, Kentucky. *International Journal of Coal Geology, 220*, 103413. https://doi.org/10.1016/j.coal.2019.103413.

Hower, J.C., Groppo, J.G., Joshi, P., Preda, D.V., Gamliel, D.P., Mohler, D.T., Wiseman, J.D., Hopps, S.D., Morgan, T.D., Beers, T., Schrock, M., (2020b). Distribution of Lanthanides, Yttrium, and Scandium in the pilot-scale beneficiation of fly ashes derived from eastern Kentucky coals. Minerals 10, 105. https://doi.org/10.3390/min10020105

Hower, J.C., Eble, C.F., Backus, J.S., Xie, P., Liu, J. Fu, B., Hood, M.M., (2020c). Aspects of Rare Earth Element enrichment in Central Appalachian coals. *Applied Geochemistry 120*, 104676. https://doi.org/10.1016/j.apgeochem.2020.104676

Hu, Y., Florek, J., Larivière, D., Fontaine, F.-G., Kleitz, F. (2018) Recent Advances in the Separation of Rare Earth Elements Using Mesoporous Hybrid Materials. *The Chemical Record*, *18*, 1261-1276.

Huang, Q., Noble, A., Herbst, J., Honaker, R. (2018). Liberation and release of rare earth minerals from Middle Kittanning, Fire Clay, and West Kentucky No. 13 coal sources. *Powder Technology, 332*, 242-252.

Ice, G.E., Budai, J.D., Pang, J.W.L. (2011) The Race to X-ray Microbeam and Nanobeam Science. *Science, 334*, 1234-1239.

International Energy Agency (2018). *World Energy Outlook 2018*. https://www.iea.org/weo2018/ (accessed 16 January 2019).

Ireland, T.R. (2014). *Ion microscopes and microprobes, section 15.21*. Treatise in Geochemistry (2nd Edition) 15, 385-409, Elsevier.

Ireland, T.R., Clement, S., Compston, W., Foster, J.J., Holden, P., Jenkins, B., Lanc, P., Schram, N., Williams, I.S. (2008). Development of SHRIMP. *Australian Journal of Earth Sciences*, *55*, 937-954.

Joshi, P.B., Preda, D.V., Skyler, D.A., Tsinberg, A., Green, B.D., Marinelli, W.J. (2013). *U.S. Patent Application Number 13/864677, Recovery of Rare Earth Elements and Compounds from Coal Ash*, in: Office, U.S.P.a.T. (Ed.).

Kaplan, S. (2020). Why coal lost – and can it recover? Power, https://www.powermag.com/why-coal-lost-and-can-it-recover/ (Accessed 31 July 2020).

Kelmers, A., Canon, R., Egan, B., Felker, L., Gilliam, T., Jones, G., Owen, G., Seeley, F., Watson, J. (1982). Chemistry of the direct acid leach, calsinter, and pressure digestion-acid leach methods for the recovery of alumina from fly ash. *Resources and Conservation, 9*, 271-279.

Keystone Coal Industry Manual (2009). *2010 Keystone Coal Industry Manual*. Jacksonville, FL, Mining Media International, 631 p.

Kim, D., Powell, L., Delmau, L., Peterson, E., Herchenroeder, J., Bhave, R. (2015). Selective extraction of rare earth elements from permanent magnet scraps with membrane solvent extraction, *Environmental Science & Technology*, *49*, 9452-9459.

King, J.F., Taggart, R.K., Smith, R.C., Hower, J.C., Hsu-Kim, H. (2018) Aqueous acid and alkaline extraction of rare earth elements from coal combustion ash. *International Journal of Coal Geology, 195*, 75-83.

Kolker, A. (2018). *Topics in coal geochemistry- Short course*. U.S. Geological Survey Open File Report 2018-1145, https://pubs.er.usgs.gov/publication/ofr20181145, https://doi.org/10.3133/ofr20181145.

Kolker, A., Scott, C., Hower, J.C., Vazquez, J.A., Lopano, C.L., Dai, S. (2017). Distribution of rare elements in coal combustion fly ash, determined by SHRIMP-RG ion microprobe. *International Journal of Coal Geology, 184*, 1–10, https://doi.org/10.1016/j.coal.2017.10.002.

Korotev, R.L. (2009). *"Rare Earth Plots" and the Concentrations of Rare Earth Elements (REE) in Chondritic Meteorites*. http://meteorites.wustl.edu/goodstuff/ree-chon.htm, accessed 25 November 2018.

Kortright, J.B., Thompson, A.C., (2009). *X-ray Emission Energies*. In: Thompson, A.C., Vaughan, D. (Eds.), X-ray Data Booklet. Lawrence Berkeley National Laboratory, Berkeley, CA, pp. 1-8 to 1-27.

Kose-Mutlu, B., Hsu-Kim, H., Wiesner, M. R. (2020). Separation of Rare Earth Elements from Mixed-Metal Feedstocks by Micelle Enhanced Ultrafiltration with Sodium Dodecyl Sulfate †. *Environmental Technology*, https://doi.org/10.1080/09593330.2020.1812732.

Kostova, I., Vassileva, C., Dai, S., Hower, J.C., (2016). Mineralogy, geochemistry and mercury content characterization of fly ashes from the Maritza 3 and Varna thermoelectric power plants, Bulgaria. *Fuel, 186*, 674-684.

Kutchko, B.G., Kim, A.G., (2006). Fly ash characterization by SEM-EDS. *Fuel, 85*, 2537-2544, doi:10.1016/j.fuel.2006.05.016.

Lichte, F.E., Meier, A.L., Crock, J.G. (1987) Determination of the rare-earth elements in geological materials by inductively coupled plasma mass spectrometry. *Analytical Chemistry, 59*, 1150-1157.

Lin, R., Bank, T.L., Roth, E.A., Granite, E.J., and Soong, Y. (2017a). Organic and inorganic associations of rare earth elements in central Appalachian coal: *International Journal of Coal Geology, 179*, 295-301.

Lin, R., Howard, B.H., Roth, E.A., Bank, T.L., Granite, E.J., Soong, Y. (2017b). Enrichment of rare earth elements from coal and coal by-products by physical separations. *Fuel, 200*, 506-520.

Lin, R., Soong, Y., Granite, E.J. **(**2018a**)**. Evaluation of trace elements in U.S. coals using the USGS COALQUAL database version 3.0. Part I: Rare earth elements and yttrium (REY). *International Journal of Coal Geology***,** 192, 1-13.

Lin, R., Stuckman, M., Howard, B.H., Bank, T.L., Roth, E.A., Macala, M.K., Lopano, C., Soong, Y., Granite, E.J. (2018b) Application of sequential extraction and hydrothermal treatment for characterization and enrichment of rare earth elements from coal fly ash. *Fuel, 232*, 124-133.

Liu, J., Dai, S., He, X., Hower, J.C., Sakulpitakphon, T. (2017). Size-dependent variations in fly ash trace-element chemistry: Examples from a Kentucky power plant and with emphasis on rare earth elements. *Energy & Fuels, 31*, 438-447. DOI: 10.1021/acs.energyfuels.6b02644.

Liu, P., Huang, R. and Tang, Y. (2019). Comprehensive understandings of Rare Earth Element (REE) speciation in coal fly ashes and implication for REE extractability. *Environmental Science & Technology*, 53(9), 5369-5377.

Lo, Y.-C., Cheng, C.-L., Han, Y.-L., Chen, B.-Y., Chang, J.-S. (2014) Recovery of high-value metals from geothermal sites by biosorption and bioaccumulation. *Bioresource Technology,* 160, 182-190.

Longerich, H. (2009). Laser ablation-inductively coupled plasma-mass spectrometry (LA-ICP-MS): an introduction. Chapter 1, in Sylvester, P., ed., Laser ablation ICP-MS in the earth sciences: Current practices and outstanding issues. *Mineralogical Association of Canada Short Course,* 40, 1-18.

McDowell, W.J., Seeley, F.G., (1981). *Salt-soda sinter process for recovering aluminum from fly ash*. US Patent 4254088A. Sandia National Laboratories (SNL), Albuquerque, NM, and Livermore, CA.

Makarova, I. , Ryl, J., Sun, Z., Kurilo, I., Gornicka, K., Laatikainen, M., Repo, E. (2020). One-step recovery of REE oxalates in electro-leaching of spent NdFeB magnets. *Separation and Purification Technology, 251,* 117362.

Mardon, S.M., Hower, J.C. **(**2004**)**. Impact of coal properties on coal combustion by-product quality: examples from a Kentucky power plant. *International Journal of Coal Geology***,** 59, 153–169.

Meawad, A.S., Bojinova, D.Y., Pelovski, Y.G. (2010). An overview of metals recovery from thermal power plant solid wastes. *Waste Management, 30*, 2548-2559.

Merriman, D., Backeberg, N. (2018). *Rare earths: Is new non-Chinese supply diversifying the industry?* Roskill Information Services, https://roskill.com/news/rare-earths-is-new-non-chinese-supply-diversifying-the-industry/ (Accessed 22 June 2020).

Middleton, A., Park, D., Jiao, Y., Hsu-Kim, H. (2020). Elemental Composition Controls Rare Earth Element Solubility During Leaching of Coal Fly Ash and Coal By-Products. *International Journal of Coal Geology*, 227, 103532.

Miller, J.W. (2015). *Molycorp to Suspend Production at California Mine; Firm, amid a price collapse for rare earths, to lay off almost 500 workers at Mountain Pass facility*. Wall Street Journal (Online), 26 August 2015. https://www.wsj.com/articles/molycorp-to-suspend-production-at-california-mine-1440616302 (Accessed 22 June 2020))

Molycorp Minerals LLC, (2010). *Revised Mine and Reclamation Plan for the Mountain Pass Mine; Draft Subsequent Mitigated Negative Declaration*. Submitted to County of San Bernardino, p. 97.

Mutlu, B.K., Cantoni, B., Turolla, A., Antonelli, M., Hsu-Kim, H., Wiesner, M.R. (2018). Application of nanofiltration for Rare Earth Elements recovery from coal fly ash leachate: Performance and cost evaluation. *Chemical Engineering Journal, 349*, 309-317.

Neuendorf, K.K.E., Mehl, J.P., Jr., Jackson, J.A. (2005). Glossary of geology (5th edition). American Geological Institute (now American Geosciences Institute). Alexandria, VA, 779 p.

O'Connor, M.P., Coulthard, R.M., Plata, D.L. (2018). Electrochemical deposition for the separation and recovery of metals using carbon nanotube-enabled filters. *Environmental Science: Water Research and Technology*, *4 (1)*, 58-66.

Oddo, G., (1914). Die Molekularstruktur der radioaktiven Atome. *Zeitschrift für anorganische Chemie, 87,* 253. doi:10.1002/zaac.19140870118.

Osborn, E.F., Muan, A. (1960). *Phase equilibrium diagrams of oxide systems. The system CaO-Al_2O_3-SiO_2. Plate 1*. The American Ceramic Society and the Edward Orton Jr. Ceramic Foundation, Columbus, Ohio.

Padilla, R., Sohn, H.Y. (1985) Sintering kinetics and alumina yield in lime-soda sinter process for alumina from coal wastes. *Metallurgical Transactions B, 16*, 385-395.

Palmer, C.A., Oman, C.L., Park, A.J., Luppens, J.A. (2015). *The U.S. Geological Survey coal quality (COALQUAL) database version 3.0.* U.S. Geological Survey Data Series 975, 43 p. with appendixes, http://dx.doi.org/10.3133/ds975.

Park, D.M., Brewer, A., Reed, D.W., Lammers, L.N., Jiao, Y. (2017) Recovery of Rare Earth Elements from Low-Grade Feedstock Leachates Using Engineered Bacteria. *Environmental Science & Technology, 51*, 13471-13480.

Park, D., Middleton, A., Smith, R., Deblonde, G., Laudal, D., Theaker, N., Hsu-Kim, H., Jiao, Y. (2020). A biosorption-based approach for selective extraction of rare earth elements from coal byproducts. *Separation and Purification Technology, 241*, 116726.

Peak Resources Limited, (2017). *Ngualla Rare Earth Project - Updated Ore Reserve*. https://wcsecure.weblink.com.au/pdf/PEK/01847311.pdf. ((Accessed 22 June 2020))

Piispanen, M. H., Arvilommi, S. A., Van Den Broeck, B., Nuutinen, L. H., Tiainen, M. S., Perämäki, P. J., Laitinen, R. S. (2009). A comparative study of fly ash characterization by LA-ICP-MS and SEM-EDS. *Energy and Fuels, 23(7),* 3451-3456. doi:10.1021/ef801037a

Quercia, G., Perera, Y., Tovar, H., Rodriguez, E. (2007). Thermal degradation of zirconium silicate ($ZrSiO_4$) ferrules. *Acta Microscopica, 16*, 205-206.

Querol, X., Chenery, S. (1995). *Determination of trace element affinities in coal by laser ablation microprobe-inductively coupled plasma mass spectrometry.* In: Whateley, M.K.G, and Spears, D.A., eds., European Coal Geology, London, Geological Society Special Publication 82, p. 147-155.

Querol, X., Moreno, N., Umaña, J.C., Alastuey, A., Hernández, E., López-Soler, A., Plana, F. (2002) Synthesis of zeolites from coal fly ash: an overview. *International Journal of Coal Geology, 50*, 413-423.

Rahman, M.M., Awual, M.R., Asiri, A.M. (2020). Preparation and evaluation of composite hybrid nanomaterials for rare-earth elements separation and recovery. *Separation and Purification Technology, 253,* 117515.

Ratafia-Brown, J.A. (1994). Overview of trace element partitioning in flames and furnaces of utility coal-fired boilers. *Fuel Processing Technology, 39*, 139–157.

Rayzman, V.L., Shcherban, S.A., Dworkin, R.S. (1997). Technology for Chemical−Metallurgical Coal Ash Utilization. *Energy & Fuels, 11*, 761-773.

Roskill Information Services (2017). *Rare earths: What's the coal story?* Roskill Information Services, https://roskill.com/news/rare-earths-whats-coal-story/ ((Accessed 22 June 2020)).

Roskill Information Services (2018). *Rare earths: African ramp-up and Australian advances for rare earth supply.* Roskill Information Services, https://roskill.com/news/rare-earths-african-ramp-up-and-australian-advances-for-rare-earth-supply/ (Accessed 22 June 2020).

Rybak, A., Rybak, A. (2021). Characteristics of some selected methods of rare earth elements recovery from coal fly ashes. *Minerals*, 11, 142.

Seredin, V.V. (1996). Rare earth element-bearing coals from the Russian Far East deposits. *International Journal of Coal Geology,* 30, 101–129.

Seredin, V.V. (2010). A new method for primary evaluation of the outlook for rare earth element ores. *Geology of Ore Deposits, 52,* 428-433.

Seredin, V.V., Dai, S. (2012). Coal deposits as potential alternative sources for lanthanides and yttrium. *International Journal of Coal Geology, 94*, 67-93.

Seydoux-Guillaume, A.M., Wirth, R., Nasdala, L., Gottschalk, M., Montel, J.M., Heinrich, W. (2002). An XRD, TEM and Raman study of experimentally annealed natural monazite. *Physics and Chemistry of Minerals, 29*, 240-253.

Silva, L.F.O., Jasper, A., Andrade, M.L., Sampaio, C.H., Dai, S., Li., X., Li, T., Chen, W., Wang, X., Liu, H., Zhao, L., Hopps, S.G., Jewell, R.F., Hower, J.C. (2012). Applied investigation on the interaction of hazardous elements binding on ultrafine and nanoparticles in Chinese anthracite-derived fly ash. *The Science of the Total Environment, 419*, 250-264.

Sloss, L. (2019). *Technology readiness of advanced coal-based power generation systems.* International Energy Agency, IEA Clean Coal Centre, CCC/ 292, 113 p.

Smith, R. C., Taggart, R. K., Hower, J. C., Wiesner, M. R., Hsu-Kim, H. (2019). Selective Recovery of Rare Earth Elements from Coal Fly Ash Leachates Using Liquid Membrane Processes. *Environmental Science & Technology, 58*(8), 4490-4499.

Smolka-Danielowska, D. (2010). Rare earth elements in fly ashes created during the coal burning process in certain coal-fired power plants operating in Poland-Upper Silesian Industrial Region. *Journal of Environmental Radioactivity 101*, 965-968 doi:10.1016/j.jenvrad.2010.07.001.

Spears, D. A. (2004). The use of laser ablation inductively coupled plasma-mass spectrometry (LA ICP-MS) for the analysis of fly ash. *Fuel, 83,* 1765-1770. doi:10.1016/j.fuel.2004.02.018

Stern, R.A., 2009. An introduction to secondary ion mass spectrometry (SIMS) in geology, Chapter 1, in Fayek, M., ed., Secondary mass spectrometry in the earth sciences: Gleaning the big picture from a small spot. *Mineralogical Association of Canada Short Course 41*, 1-18.

Stuckman, M.Y., Lopano, C.L., Granite, E.J. (2018). Distribution and speciation of rare earth elements in coal combustion by-products via synchrotron microscopy and spectroscopy. *International Journal of Coal Geology, 195*, 125-138.

Suárez-Ruiz, I., Valentim, B., Borrego, A.G., Bouzinos, A., Flores, D., Kalaitzidis, S., Malinconico, M.L., Marques, M., Misz-Kennan, M., Predeanu, G., Montes, J.R., Rodrigues, S., Siavalas, G., Wagner, N. (2017). Development of a petrographic classification of fly-ash components from coal combustion and co-combustion. (An ICCP Classification System, Fly-Ash Working Group – Commission III.). *International Journal of Coal Geology, 183*, 188-203. DOI: 10.1016/j.coal.2017.06.004

Sylvester, P., ed., (2001). *Laser-Ablation ICP-MS in the Earth Sciences: Principles and Applications*. Mineralogical Association of Canada Short Course Series, 29, 243 p.

Sylvester P., ed., (2008). *Laser Ablation ICP-MS in the Earth Sciences: Current Practices and Outstanding Issues.* Mineralogical Association of Canada Short Course Series, 40, 356 p.

Taggart, R.K., Hower, J.C., Dwyer, G.S., Hsu-Kim, H. (2016). Trends in the Rare Earth Element Content of U.S.-Based Coal Combustion Fly Ashes. *Environmental Science & Technology, 50,* 5919-5926.

Taggart, R.K., Hower, J.C., Hsu-Kim, H. (2018a). Effects of Roasting Additives and Leaching Parameters on Extraction of Rare Earth Elements from Coal Fly Ash. *International Journal of Coal Geology, 196,* 106-114.

Taggart, R.K., Rivera, N.A., Levard, C., Ambrosi, J.-P., Borschneck, D., Hower, J.C., Hsu-Kim, H. (2018b). Differences in bulk and microscale yttrium speciation in coal combustion fly ash. *Environmental Science: Processes & Impacts, 20*, 1390-1403.

Taylor, S.R. McLennan, S.M., (1985). *The Continental Crust—Its Composition and Evolution*. Boston, Blackwell Scientific Publishers, 312 p.

Thomas, R. (2013). *Practical Guide to ICP-MS; A Tutorial for Beginners.* Third Edition. CRC Press, Boca Raton, FL.

Thompson, R. L., Bank, T., Montross, S., Roth, E., Howard, B., Verba, C., Granite, E. (2018). Analysis of rare earth elements in coal fly ash using laser ablation inductively coupled plasma mass spectrometry and scanning electron microscopy. *Spectrochimica Acta - Part B Atomic Spectroscopy*, 143, 1-11. doi:10.1016/j.sab.2018.02.009

Thompson, R.L., Bank, T., Roth, E., Granite, E. (2016) Resolution of rare earth element interferences in fossil energy by-product samples using sector-field ICP-MS. *Fuel, 185*, 94-101.

U.S. Department of Energy, National Energy Technology Laboratory. (2018). *Rare earth elements from coal and coal byproducts.* https://www.netl.doe.gov/research/coal/rare-earth-elements.

U.S. Geological Survey. (2014). *The rare-earth elements-Vital to modern technologies and lifestyles*. U.S. Geological Survey Fact Sheet 2014-3078, 4 p., https://pubs.usgs.gov/fs/2014/3078/. (Accessed 22 June 2020)

Valentim, B. (2020). Petrography of coal combustion char: A review. *Fuel, 277,* 118271.

Valentim, B., Hower, J.C., Soares, S., Guedes, A., Garcia, C., Flores, D., Oliveira, Á. (2009). Petrographic characterization of economizer fly ash. *Minerals and Metallurgical Processing, 26*, 208-216.

Wang, Z., Dai, S., Zou, J., French, D., & Graham, I. T. (2019). Rare earth elements and yttrium in coal ash from the Luzhou power plant in Sichuan, Southwest China: Concentration, characterization and optimized extraction. *International Journal of Coal Geology*, 203, 1-14.

Ward, C.R., French, D. (2006). Determination of glass content and estimation of glass composition in fly ash using quantitative X-ray diffractometry. *Fuel, 85*, 2268-2277, doi:10.1016/j.fuel.2005.12.026.

Watson, B., (2018). Rare earth hunting in US coal country. *Defense One Radio*, 18 October 2018, https://www.stitcher.com/podcast/defense-one-radio/e/56804885?refid=stpr&autoplay=true (starts at 28:50), (accessed 17 June 2020).

Wilcox, J., Wang, B., Rupp, E., Taggart, R., Hsu-Kim, H., Oliveira, M.L.S., Cutruneo, C.M.N.L., Taffarel, S., Silva, L.F.O., Hopps, S.D., Thomas, G.A., Hower, J.C. (2015). Observations and assessment of fly ashes from high-sulfur bituminous coals and blends of high-sulfur bituminous and subbituminous coals: Environmental processes recorded at the macro and nanometer scale. *Energy & Fuels, 29*, 7168-7177. 10.1021/acs.energyfuels.5b02033.

Williams, G.P., (2009). *Electron Binding Energies*. In: Thompson, A.C., Vaughan, D. (Eds.), X-Ray Data Booklet. Lawrence Berkeley National Laboratory, Berkeley, CA, pp. 1-1 to 1-7.

World Energy Council. (2016). *World Energy Resources: Coal*. London, World Energy Council, 61-63. https://www.worldenergy.org/wp-content/uploads/2017/03/WEResources_Coal_2016.pdf.

Wraich, A. (2017). The feasibility of scandium as an expanding commodity. *Geological Society of America Annual Meeting, Seattle, Washington, paper no. 65-20*, https://gsa.confex.com/gsa/2017AM/webprogram/Paper293861.html ((Accessed 22 June 2020)).

Wright, W. (2018). *See 30 years of strip mining spread across Eastern Kentucky in mere seconds*. Lexington Herald-Leader, 30 July 2018, https://www.kentucky.com/news/state/article215487870.html ((Accessed 22 June 2020)).

Yakaboylu, G. A., Baker, D., Wayda, B., Sabolsky, K., Zondlo, J. W., Shekhawat, D., Wildfire, C., Sabolsky, E. M. (2019). Microwave-Assisted Pretreatment of Coal Fly Ash for Enrichment and Enhanced Extraction of Rare-Earth Elements. *Energy & Fuels*, 33(11), 12083-12095.

Yan, X., Dai, S., Graham, I.T., He, X., Shan, K., Liu, X. (2018) Determination of Eu concentrations in coal, fly ash and sedimentary rocks using a cation exchange resin and inductively coupled plasma mass spectrometry (ICP-MS). *International Journal of Coal Geology, 191*, 152-156.

Yang, J., Zhao, Y., Zyryanov, V., Zhang, J., Zheng, C. (2014). Physical-chemical characteristics and elements enrichment of magnetospheres from coal fly ashes. *Fuel, 135*, 15-26.

Zhang, W., Groppo, J.G., Honaker, R.Q. (2015). *Ash beneficiation for REE recovery*. World of Coal Ash, 5-7 May 2015, Nashville, TN, paper 194-Groppo-2015, http://www.flyash.info/ ((Accessed 22 June 2020)).

Zhang, W., Honaker, R.Q. (2018). Rare earth elements recovery using staged precipitation from a leachate generated from coarse coal refuse. *International Journal of Coal Geology, 195*, 189-199. DOI: 10.1016/j.coal.2018.06.008

Zhang, W., Yang, X., Honaker, R.Q. (2018). Association characteristic study and preliminary recovery investigation of rare earth elements from Fire Clay seam coal middlings. *Fuel, 215*, 551-560. DOI: 10.1016/j.fuel.2017.11.075.

Zhang, W., Noble, A., Yang, X., Honaker, R. (2020). A Comprehensive Review of Rare Earth Elements Recovery from Coal-Related Materials. *Minerals, 10*(5), 451.

Zhao, L., Dai, S., Graham, I.T., Li, X., Liu, H., Song, X., Hower, J.C., Zhou, Y. (2017). Cryptic sediment-hosted critical element mineralization from eastern Yunnan Province, southwestern China: Mineralogy, geochemistry, relationship to Emeishan alkaline magmatism and possible origin. *Ore Geology Reviews, 80,* 116–140, doi: 10.1016/j.oregeorev.2016.06.014.

Figure captions

1. Plots showing how REE data are represented, including distributions for: 1) fly ash from a Kentucky power station burning Appalachian Basin Fire Clay coal (fly ash), data from Taggart et al. (2016); 2) the upper continental crust (UCC), data from Taylor and McLennan (1985); 3) U.S. coal in USGS COALQUAL database (coal), data from Finkelman (1993); and 4) chondrite normalizing values (chondrite), as suggested by Korotev (2009). Plots show how normalization of REE concentration data results in smooth patterns for distribution for elements plotted in order of atomic number.
A. REE concentration data in parts per million showing a sawtooth pattern with even-atomic-numbered elements (Ce, Nd, Sm, Gd, Dy, Er, and Yb) more abundant than odd-numbered elements (Pr, Eu, Tb, Ho, Tm, and Lu) due to the Oddo-Harkins effect. Promethium (Pm, atomic number 61) is omitted because it is not stable in nature.
B. REE normalized to upper continental crust (UCC). Plot shows that REE distribution of fly ash and coal nearly parallel UCC, with greatest REE enrichment in fly ash. REE in coal are less than in UCC.
C. REE normalized to chondrite showing similar patterns for fly ash, UCC, and coal, with each showing enrichment in light rare earths relative to chondrite. The prominent dip in the patterns at europium (Eu, atomic number 63), is a europium anomaly (see text). Chondrite lacks this Eu anomaly. A chondrite-normalized plot is used later in this chapter.

2. Coal-derived carbons from the combustion of eastern US bituminous coals. A/ Inertinite (i) and anisotropic coke (ac). Image MD PR 01. B/ Inertinite (i), isotropic coke (ic), and anisotropic coke (ac). Image 93902 11.
C/ US San Juan Basin subbituminous coal-derived char. Image 92922 04 from Hower et al. (2017a).
D/ Chinese Yunnan anthracite-derived carbon. Image Yunnan 2 02 from Silva et al. (2012).

3. Glassy fly ash particles from the combustion of eastern US bituminous coals. A/ Glass cenospheres. Image 93685 06. B/ Particle with glass and dark, partially vitrified shale or silt bands. Image MD PS 10.

4. Spinel minerals from the combustion of eastern US bituminous coals. A/ Spinel forms in a bottom ash. Image 93662 01. B/ Spinels in fly ash. Image 93614 04. C/ Spinel from a bottom ash. Image 93933 08.

5. Stoker combustion ash from the burning of eastern US bituminous coals. Much of the left portion of the image, the triangular lower right areas, and the “bubble” in the upper right are void spaces. Much of the rest of the particle is packed with varying densities of mullite crystals in a glassy matrix. The left, rounded edge of the particle has an oxidation rim. Image 93962 06 from Hower et al. (2018a).

6. A/ Monazite (m) with glassy particles in an eastern US bituminous coal-derived fly ash. Image 93954 04 from Hood et al. (2017). B/ Zircon (z) in fly ash from Powder River Basin subbituminous coal-derived fly ash. Image 93971 02.

7. Chondrite-normalized plot of SHRIMP-RG results for constituents of a fly ash sample derived from Appalachian Basin Fire Clay coal. Figure is modified after Kolker et al. (2017). Bulk REE

distribution (heavy solid line) is from Taggart and others (2016). Plot demonstrates the relative enrichment of REE in Fe-bearing aluminosilicate glass relative to Fe-poor glasses. Quartz shows relative REE depletion or is below detection. Promethium (Pm, atomic number 61) is omitted because it is not stable in nature.

8. A/ Mixed monazite (mz) and kaolinite (k) grain in Fire Clay coal. B/ The EDX scan shows the segregation of the kaolinite (Al and Si) from the monazite (using Ce as a proxy for the REE in monazite). After Hower et al. (2018c).

9. Monazite with included xenotime in the fly ash from the combustion of an Eastern US bituminous coal blend. After Hower et al. (2017b).

10. Ce-phosphate on mullite in stoker ash from the combustion of an Eastern US bituminous coal blend. After Hower et al. (2018a).

11. Opposing sides and different sizes of the FIB liftout slice (A & B). C/ EDX image for Y, La, and Ce showing the diffuse nature of the REE distribution. From Hood et al. (2017).

12. A/ TEM image of Fe-spinel minerals (sp) in fly ash from the combustion of an Eastern US bituminous coal blend. B/ Composite EDX image based on the elements mapped individually in (C). After Hower et al. (2017b).

13. A/ TEM image of spinel (sp) surrounded by carbon. The area scanned by EDX is shown by the rectangle on the lower right of (A). The fly ash is from the combustion of an eastern US bituminous coal blend. B/ EDX scan of area shown on (A), indicating that the carbon deposit on the surface of the spinels includes/entrains Nd, Ce, Sm, and Y. After Hower et al. (2017b).

14. High resolution TEM image (right) of Al-Si glass sphere surrounded by graphitic carbon deposits. The fly ash is from the combustion of an eastern US bituminous coal blend. The composite of 50 EDX scans (left) indicates that the carbon contains Ce, Nd, Sm, and Y. After Hower et al. (2017b).

15. High resolution TEM image (upper left) of Al-Si glass sphere surrounded by graphitic carbon deposits. EDX images of C, Nd, and Ce are shown in the upper right, lower left, and lower right images, respectively. The EDX C overlapping the Al-Si glass is blacked out on the upper right image, concealing the basis for the dense Nd and Ce concentrations coincident with the glass. The fly ash is from the combustion of an Eastern US bituminous coal blend. After Hower et al. (2017b).

16. EELS imaging indicating the presence of Ce associated with needle-shaped minerals (in circles). The fly ash is from the combustion of an eastern US bituminous coal blend. After Hower et al. (2017b).

17. Example sequence of unit processes for the recovery and separation of rare earth elements at conventional mining operations (top schematic) and potential modifications to the recovery process for REE-enriched coal fly ash (bottom schematic).

Table 1. Rare earth elements in coal fly ash that could be analyzed for bulk speciation by X-ray absorption spectroscopy and potential interfering elements to consider in coal fly ash. The concentration values (from Taggart et al., 2016) correspond to fly ashes generated from coals of the central Appalachian basin in the U.S. (generally the more enriched of U.S. coal fly ashes). Fly ash samples are also enriched in other elements with absorption or emission energies that could interfere with the target element energies (Kortright and Thompson, 2009; Williams, 2009).

Element	**Concentration in fly ash**	**Absorption energy**	**Emission energy**	**Potential interfering elements**
Cerium (Ce)	100 – 200 mg kg^{-1}	5732 eV (L_3-edge)	4840.2 eV ($L\alpha_1$)	V, Ba
Lanthanum (La)	70 – 110 mg kg^{-1}	5483 eV (L_3-edge)	4651.0 eV ($L\alpha_1$)	Ti
Neodymium (Nd)	60 – 90 mg kg^{-1}	6208 eV (L_3-edge)	5230.4 eV ($L\alpha_1$)	Possibly Ce
Yttrium (Y)	80 – 100 mg kg^{-1}	17038 eV (K-edge)	14958 eV ($L\alpha_1$)	None likely

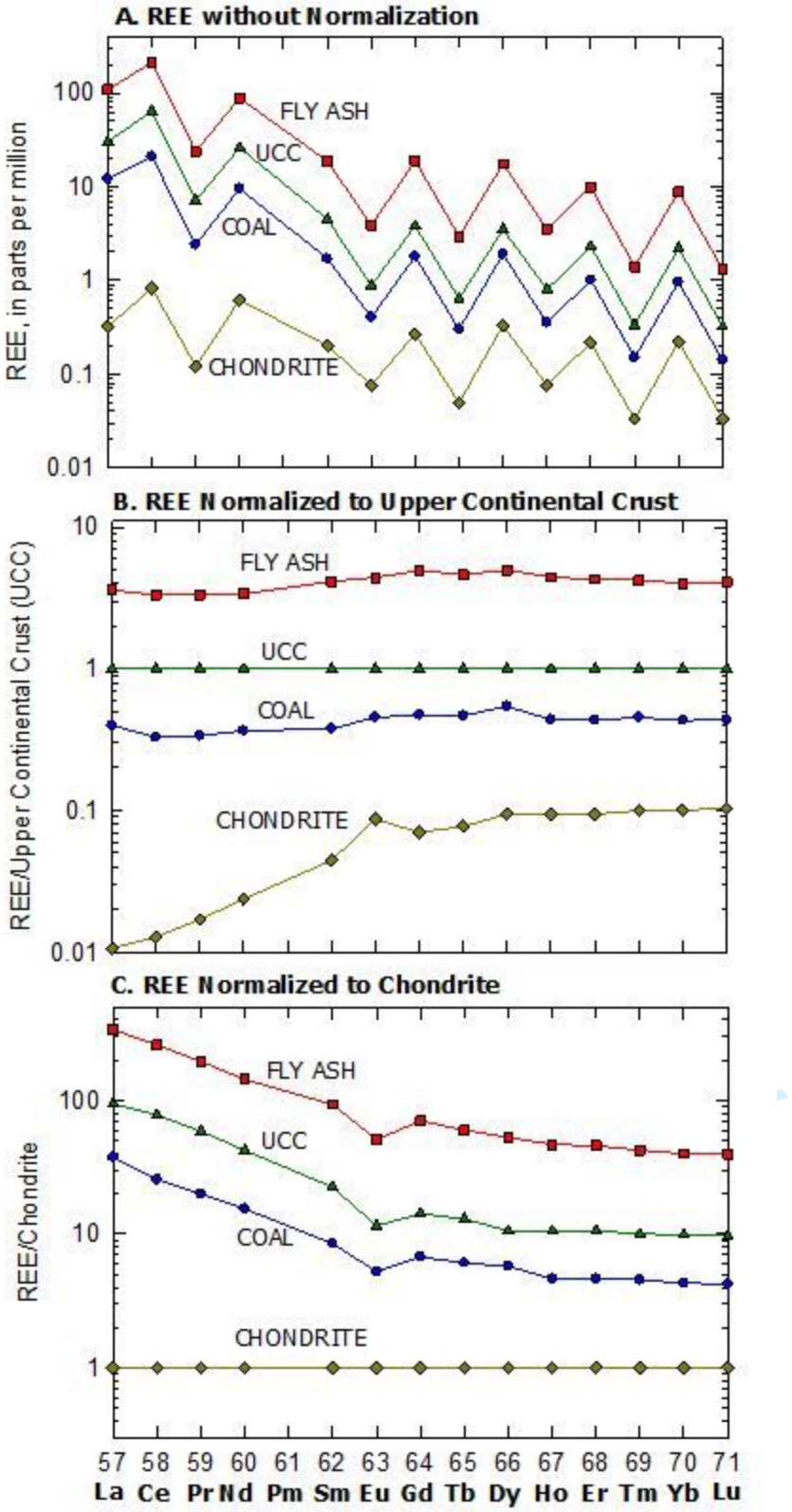

Figure 1. Plots showing how REE data are represented, including distributions for: 1) fly ash from a Kentucky power station burning Appalachian Basin Fire Clay coal (fly ash), data from

Taggart et al. (2016); 2) the upper continental crust (UCC), data from Taylor and McLennan (1985); 3) U.S. coal in USGS COALQUAL database (coal), data from Finkelman (1993); and 4) chondrite normalizing values (chondrite), as suggested by Korotev (2009). Plots show how normalization of REE concentration data results in smooth patterns for distribution for elements plotted in order of atomic number.

A. REE concentration data in parts per million showing a sawtooth pattern with even-atomic-numbered elements (Ce, Nd, Sm, Gd, Dy, Er, and Yb) more abundant than odd-numbered elements (Pr, Eu, Tb, Ho, Tm, and Lu) due to the Oddo-Harkins effect. Promethium (Pm, atomic number 61) is omitted because it is not stable in nature.

B. REE normalized to upper continental crust (UCC). Plot shows that REE distribution of fly ash and coal nearly parallel UCC, with greatest REE enrichment in fly ash. REE in coal are less than in UCC.

C. REE normalized to chondrite showing similar patterns for fly ash, UCC, and coal, with each showing enrichment in light rare earths relative to chondrite. The prominent dip in the patterns at europium (Eu, atomic number 63), is a europium anomaly (see text). Chondrite lacks this Eu anomaly. A chondrite-normalized plot is used later in this chapter.

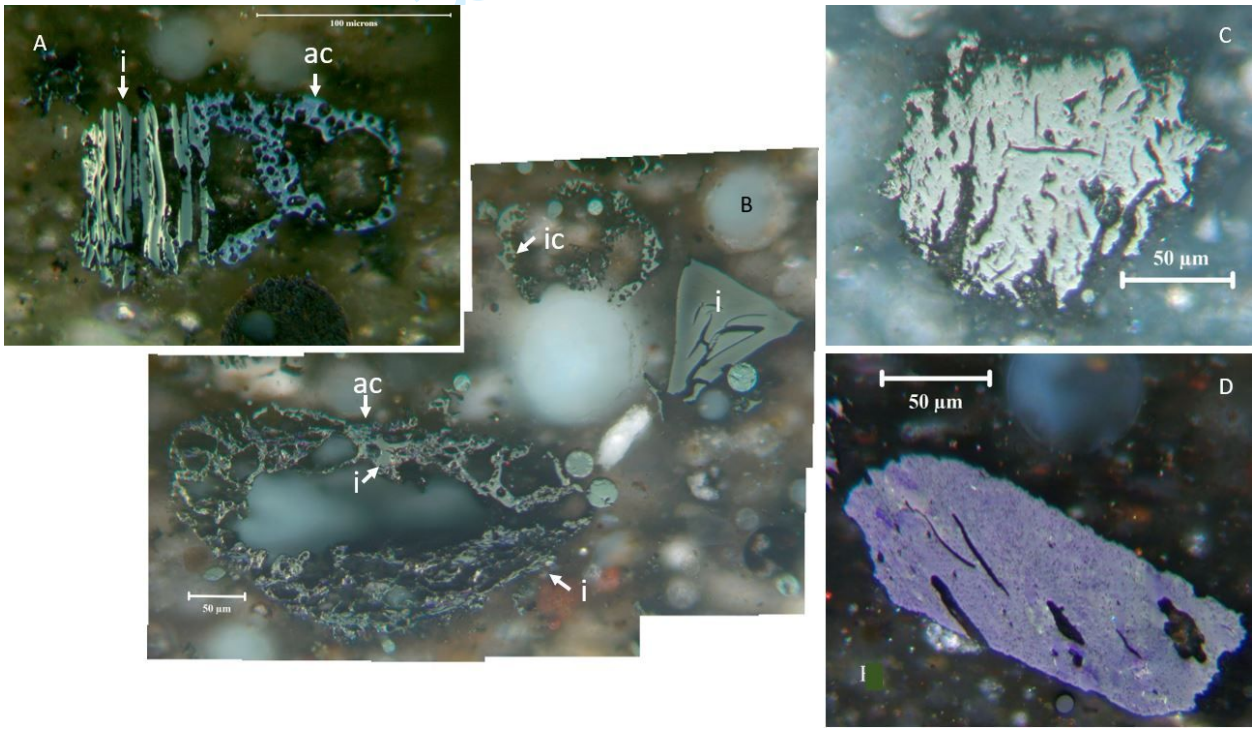

Figure 2. Coal-derived carbons from the combustion of Eastern US bituminous coals. A/ Inertinite (i) and anisotropic coke (ac). Image MD PR 01. B/ Inertinite (i), isotropic coke (ic), and anisotropic coke (ac). Image 93902 11.

C/ US San Juan Basin subbituminous coal-derived char. Image 92922 04 from Hower et al. (2017a).

D/ Chinese Yunnan anthracite-derived carbon. Image Yunnan 2 02 from Silva et al. (2012).

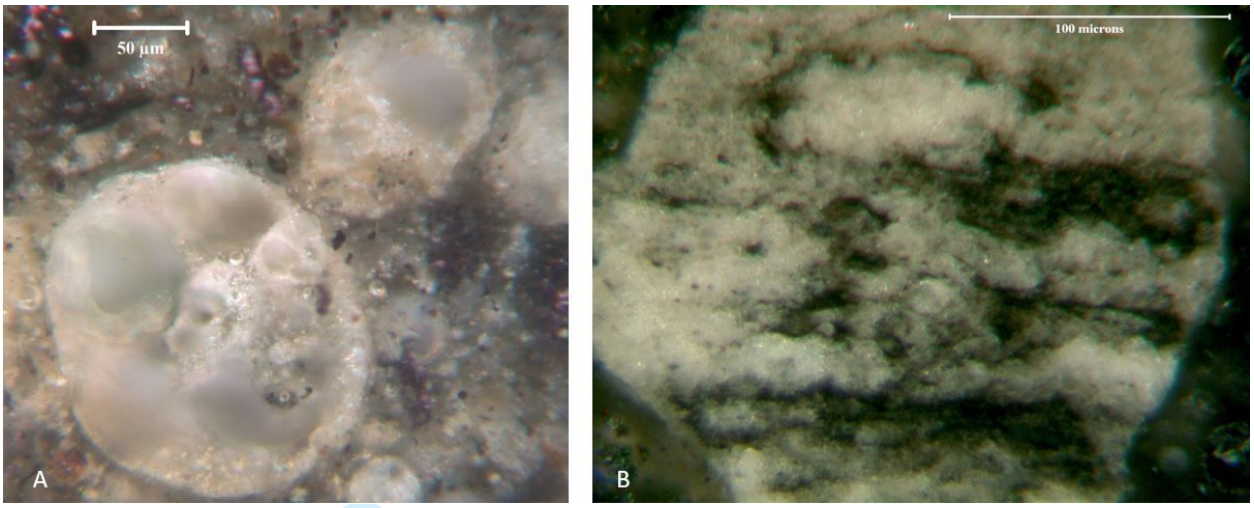

Figure 3. Glassy fly ash particles from the combustion of Eastern US bituminous coals. A/ Glass cenospheres. Image 93685 06. B/ Particle with glass and dark, partially vitrified shale or silt bands. Image MD PS 10.

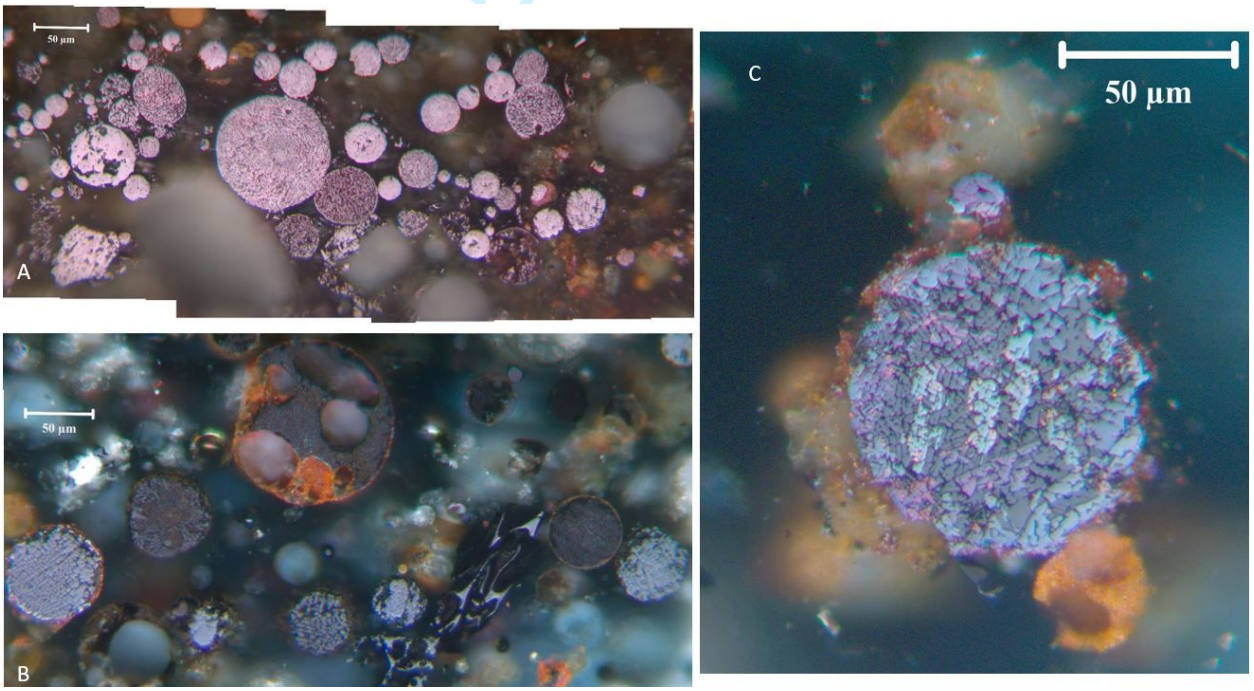

Figure 4. Spinel minerals from the combustion of Eastern US bituminous coals. A/ Spinel forms in a bottom ash. Image 93662 01. B/ Spinels in fly ash. Image 93614 04. C/ Spinel from a bottom ash. Image 93933 08.

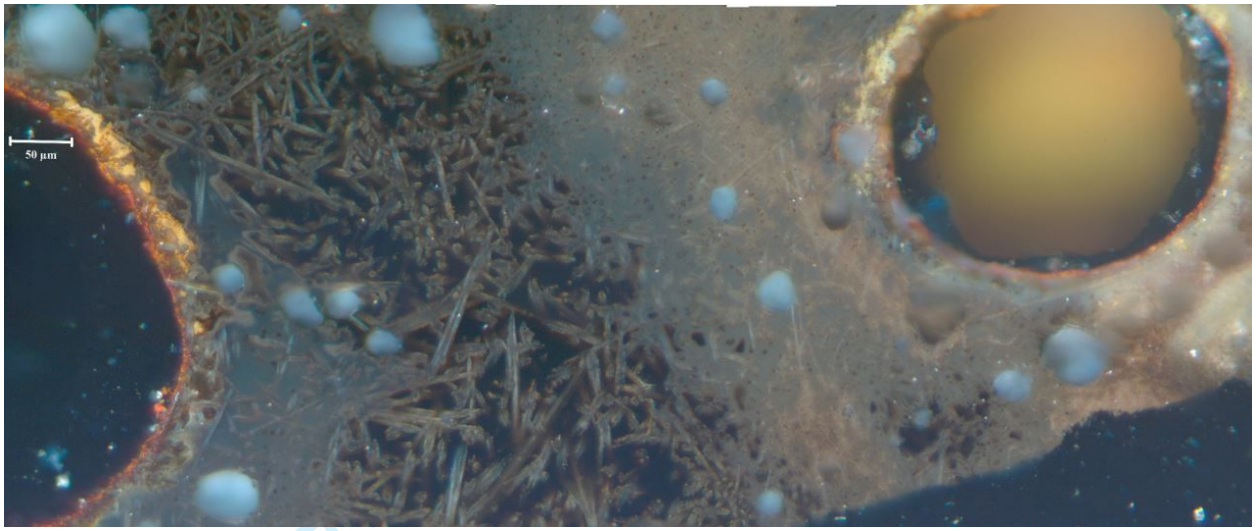

Figure 5. Stoker combustion ash from the burning of Eastern US bituminous coals. Much of the left portion of the image, the triangular lower right areas, and the "bubble" in the upper right are void spaces. Much of the rest of the particle is packed with varying densities of mullite crystals in a glassy matrix. The left, rounded edge of the particle has an oxidation rim. Image 93962 06 from Hower et al. (2018a).

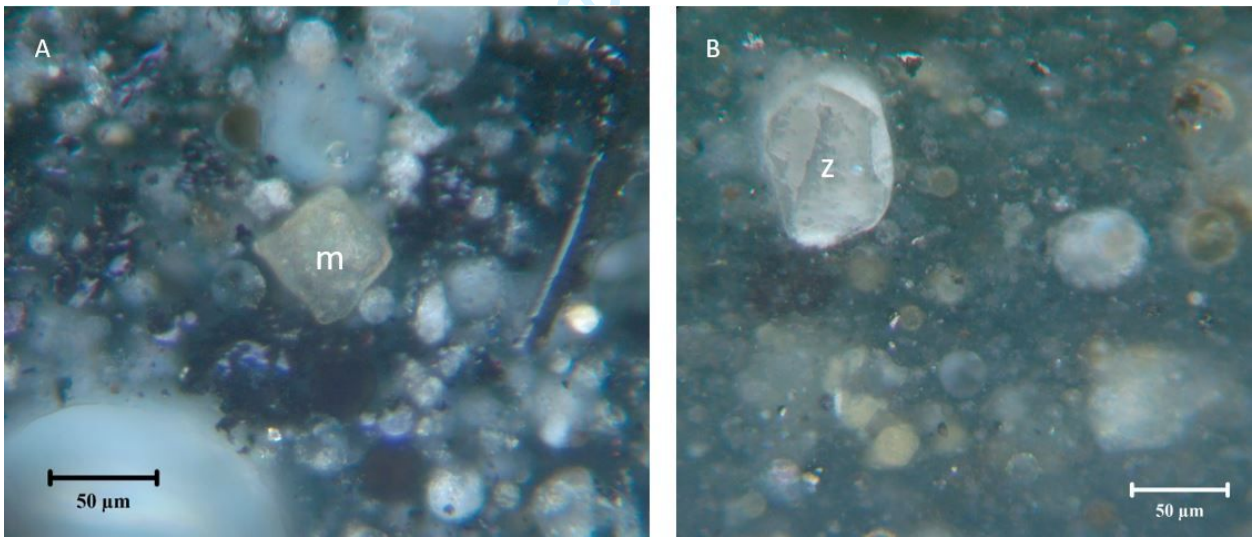

Figure 6. A/ Monazite (m) with glassy particles in an Eastern US bituminous coal-derived fly ash. Image 93954 04 from Hood et al. (2017). B/ Zircon (z) in fly ash from Powder River Basin subbituminous coal-derived fly ash. Image 93971 02.

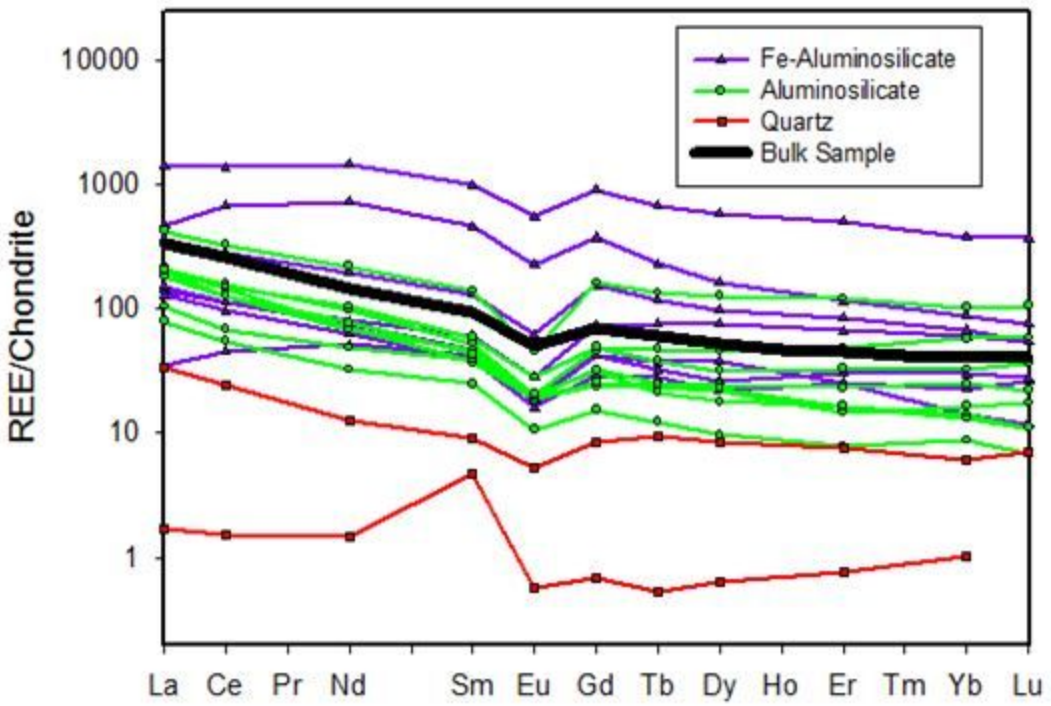

Figure 7. Chondrite-normalized plot of SHRIMP-RG results for constituents of a fly ash sample derived from Appalachian Basin Fire Clay coal. Figure is modified after Kolker et al. (2017). Bulk REE distribution (heavy solid line) is from Taggart and others (2016). Plot demonstrates the relative enrichment of REE in Fe-bearing aluminosilicate glass relative to Fe-poor glasses. Quartz shows relative REE depletion or is below detection. Promethium (Pm, atomic number 61) is omitted because it is not stable in nature.

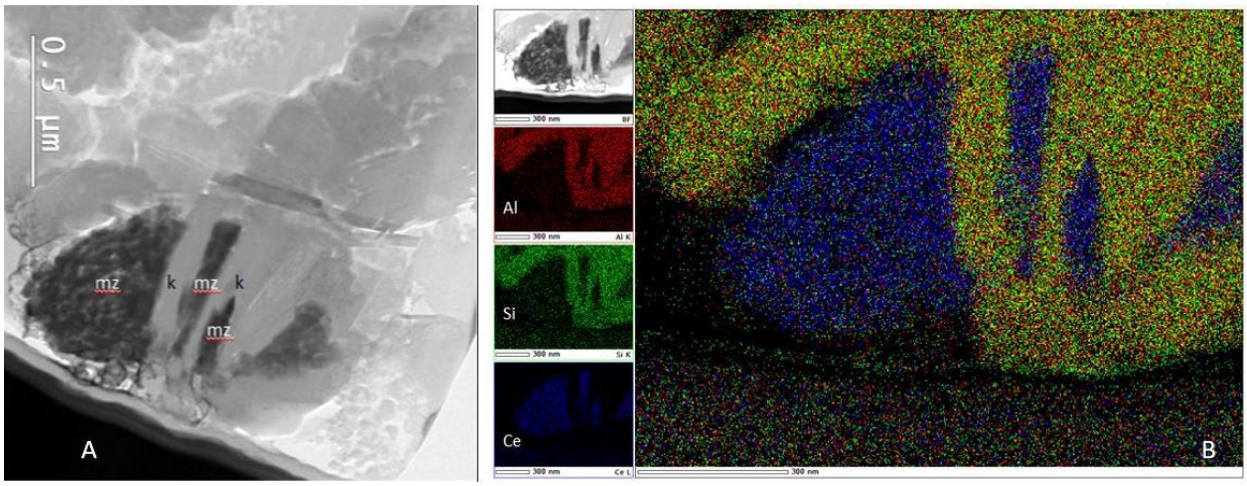

Figure 8. A/ Mixed monazite (mz) and kaolinite (k) grain in Fire Clay coal. B/ The EDX scan shows the segregation of the kaolinite (Al and Si) from the monazite (using Ce as a proxy for the REE in monazite). After Hower et al. (2018c).

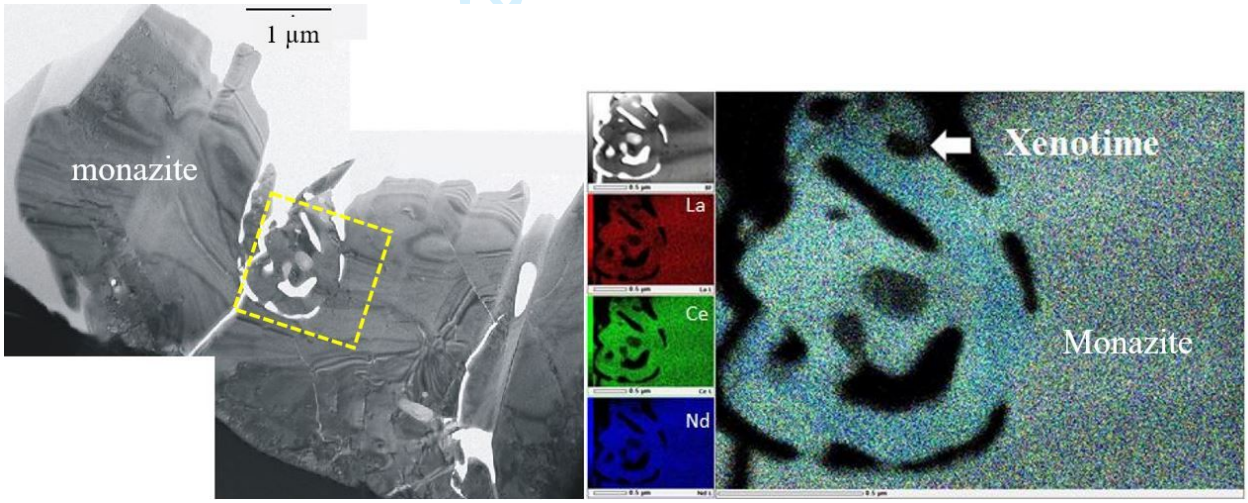

Figure 9. Monazite with included xenotime in the fly ash from the combustion of an Eastern US bituminous coal blend. After Hower et al. (2017b).

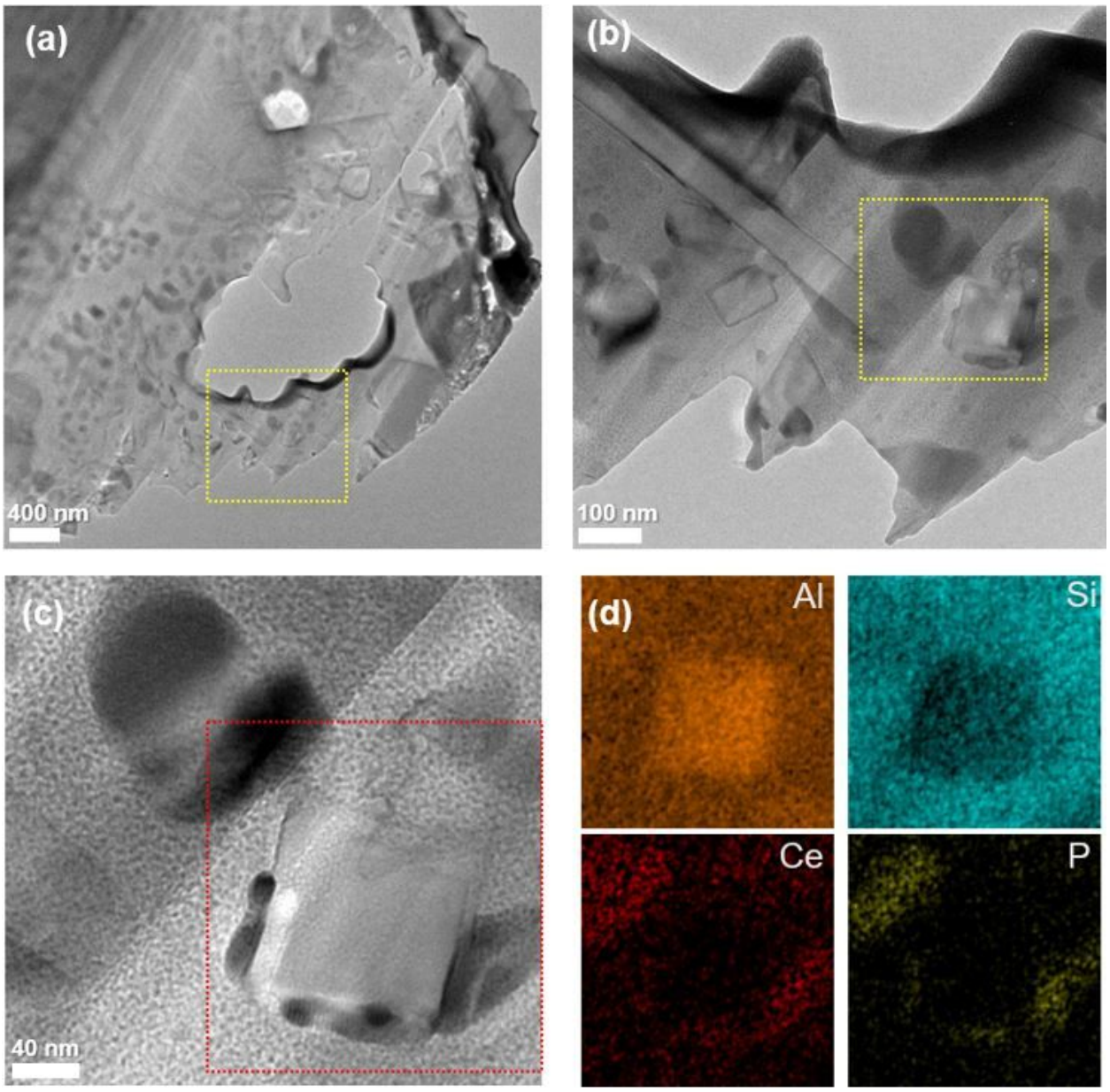

Figure 10. Ce-phosphate on mullite in stoker ash from the combustion of an Eastern US bituminous coal blend. After Hower et al. (2018a).

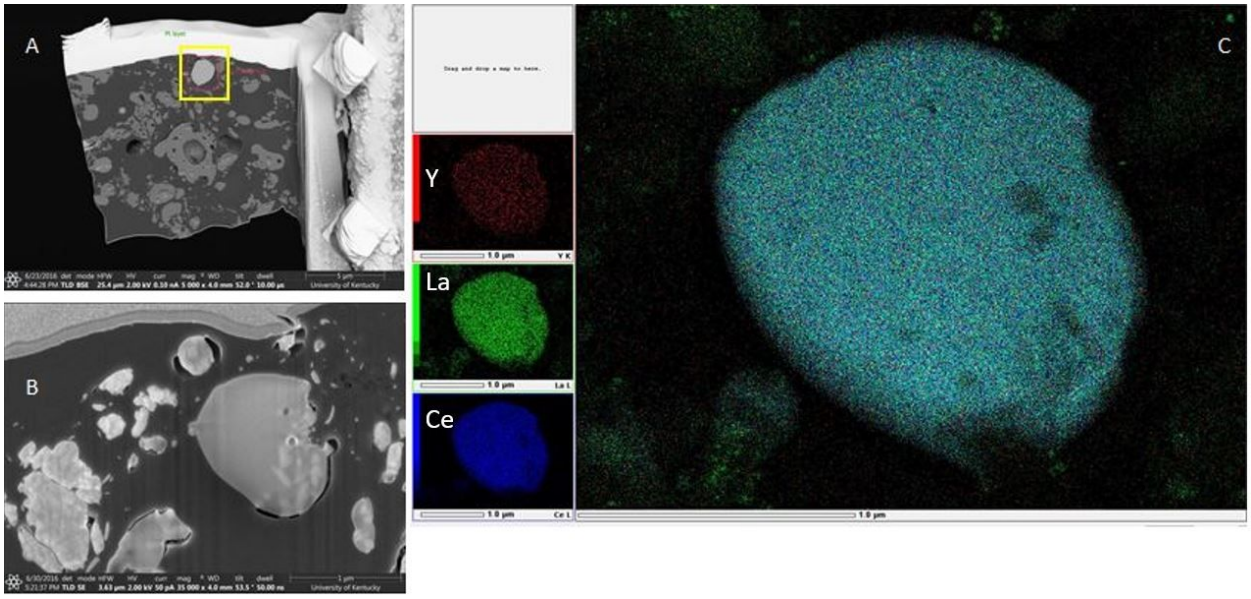

Figure 11. Opposing sides and different sizes of the FIB liftout slice (A & B). C/ EDX image for Y, La, and Ce showing the diffuse nature of the REE distribution. From Hood et al. (2017).

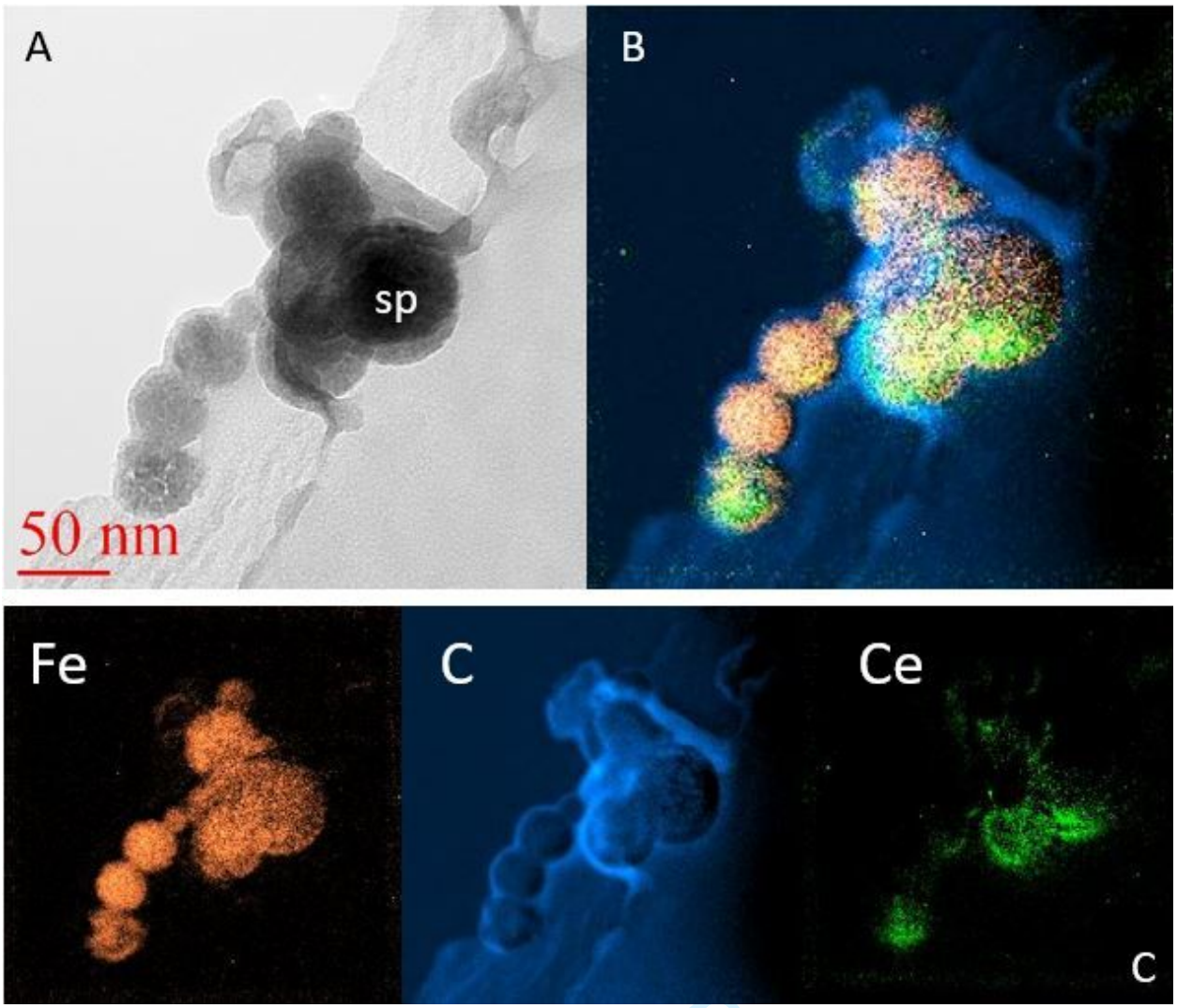

Figure 12. A/ TEM image of Fe-spinel minerals (sp) in fly ash from the combustion of an Eastern US bituminous coal blend. B/ Composite EDX image based on the elements mapped individually in (C). After Hower et al. (2017b).

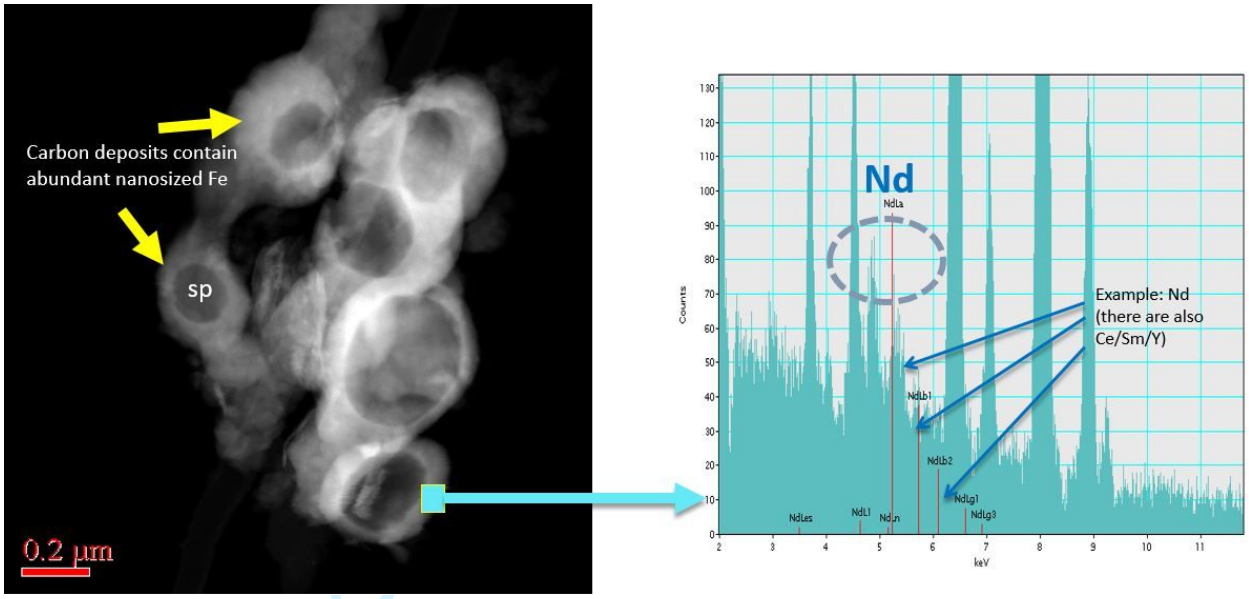

Figure 13. A/ TEM image of spinel (sp) surrounded by carbon. The area scanned by EDX is shown by the rectangle on the lower right of (A). The fly ash is from the combustion of an Eastern US bituminous coal blend. B/ EDX scan of area shown on (A), indicating that the carbon deposit on the surface of the spinels includes/entrains Nd, Ce, Sm, and Y. After Hower et al. (2017b).

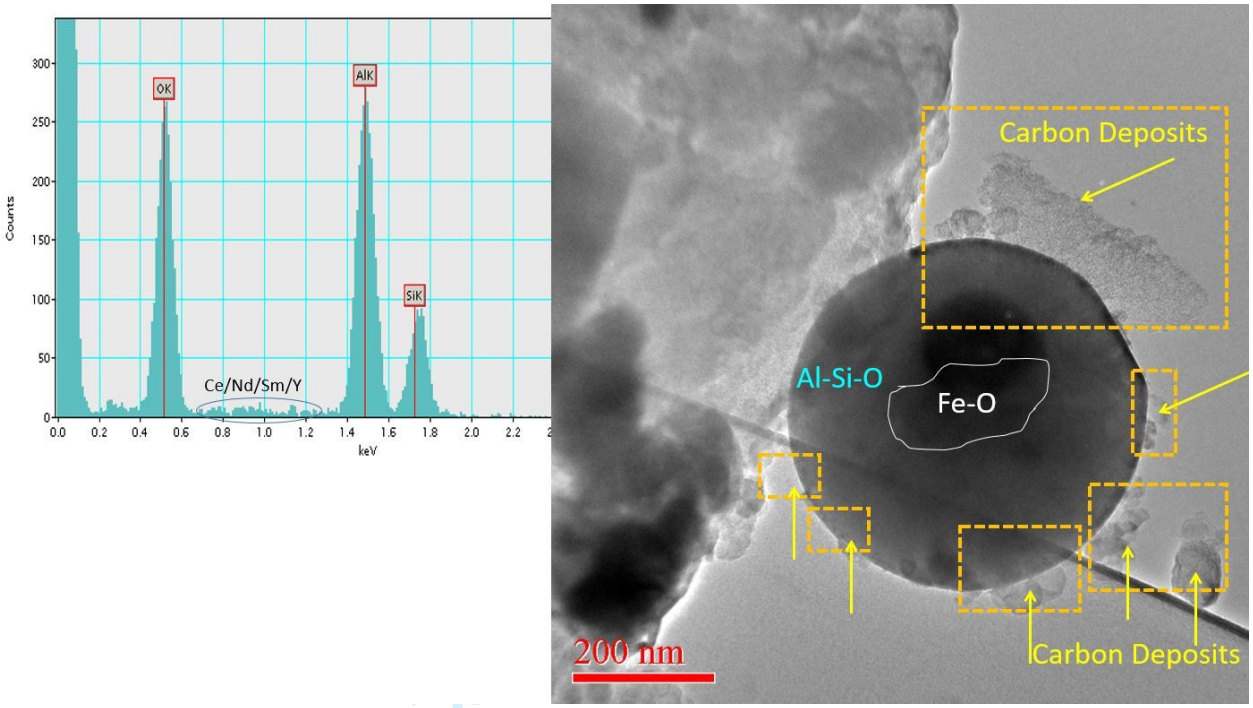

Figure 14. High resolution TEM image (right) of Al-Si glass sphere surrounded by graphitic carbon deposits. The fly ash is from the combustion of an Eastern US bituminous coal blend. The composite of 50 EDX scans (left) indicates that the carbon contains Ce, Nd, Sm, and Y. After Hower et al. (2017b).

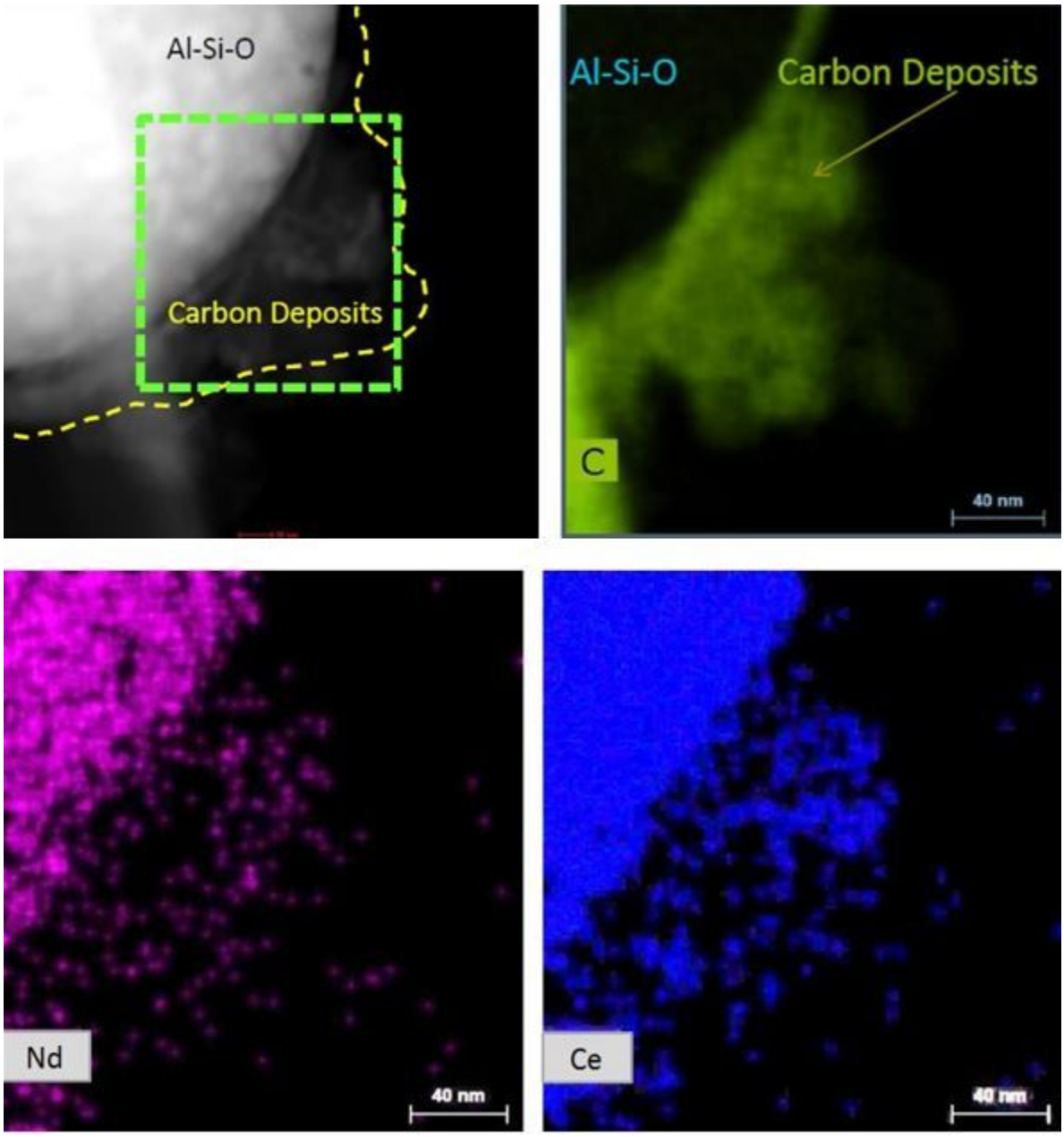

Figure 15. High resolution TEM image (upper left) of Al-Si glass sphere surrounded by graphitic carbon deposits. EDX images of C, Nd, and Ce are shown in the upper right, lower left, and lower right images, respectively. The EDX C overlapping the Al-Si glass is blacked out on the upper right image, concealing the basis for the dense Nd and Ce concentrations coincident with the glass. The fly ash is from the combustion of an Eastern US bituminous coal blend. After Hower et al. (2017b).

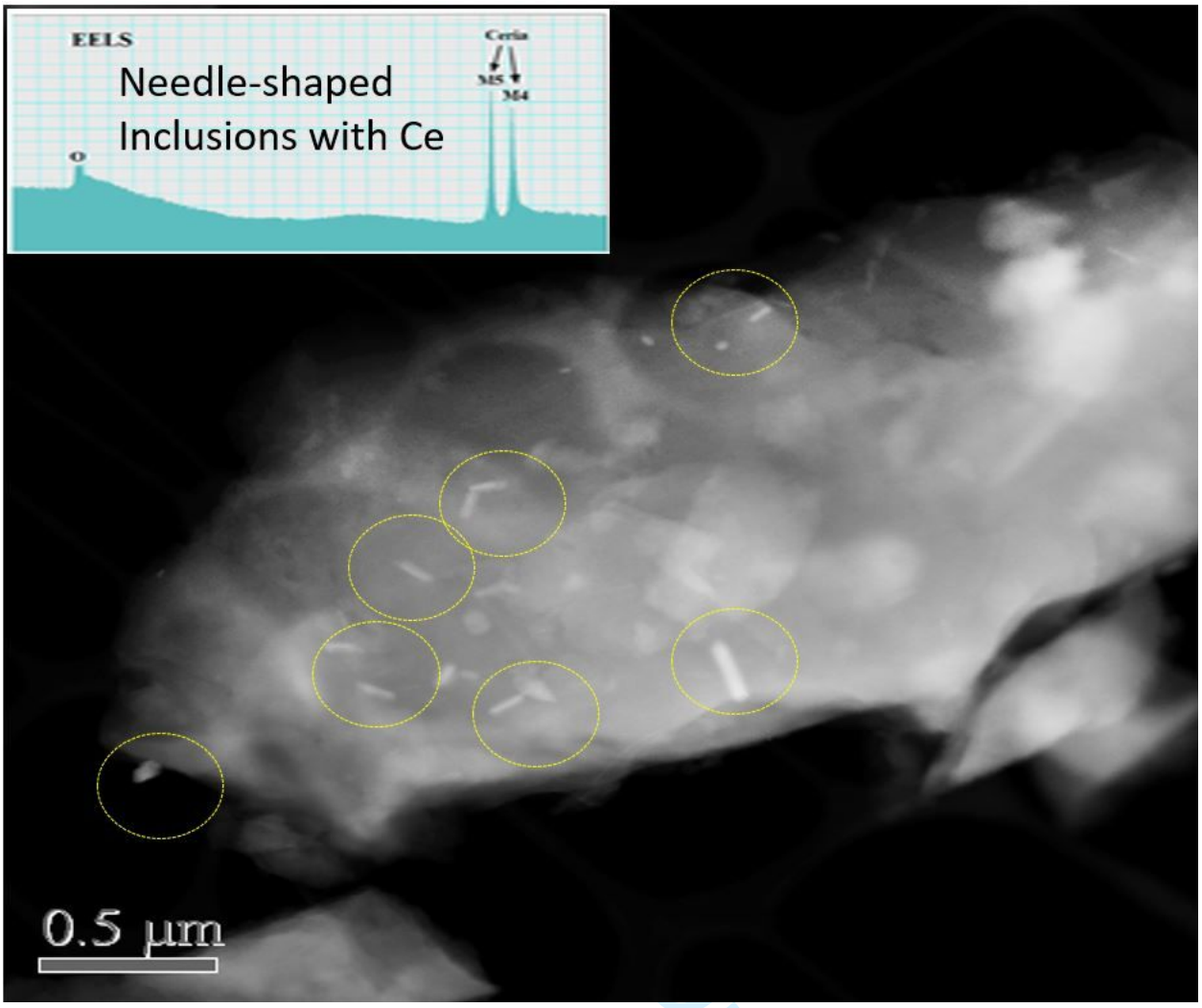

Figure 16. EELS imaging indicating the presence of Ce associated with needle-shaped minerals (in circles). The fly ash is from the combustion of an Eastern US bituminous coal blend. After Hower et al. (2017b).

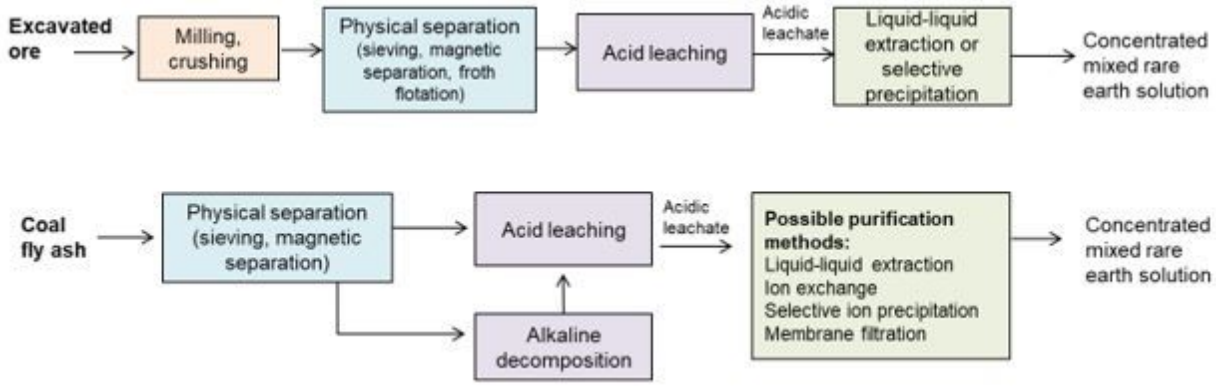

Figure 17. Example sequence of unit processes for the recovery and separation of rare earth elements at conventional mining operations (top schematic) and potential modifications to the recovery process for REE-enriched coal fly ash (bottom schematic).

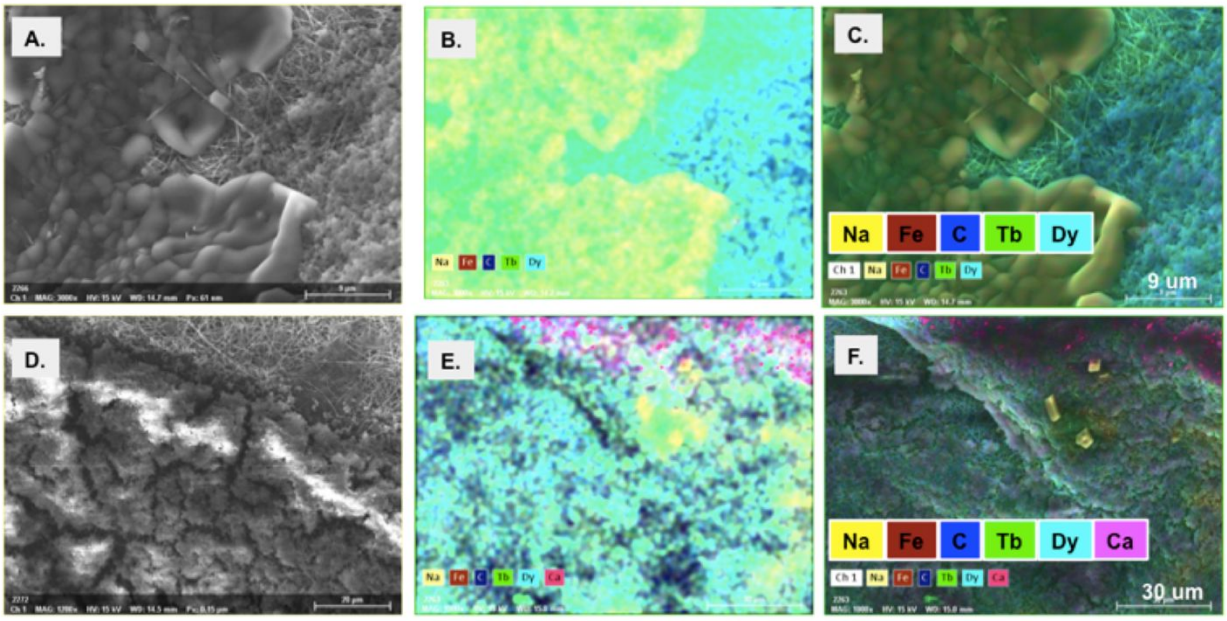

Figure 18. Scanning electron micrograph with energy dispersive x-ray spectroscopy (SEM-EDS) of rare earth elements separated from coal ash leachate using electrochemical deposition on carbon nanotube filters. Pre-treatments included an alkaline sintering of the coal ash, followed by a nitric acid extract and a pH titration using sodium hydroxide. Residual sodium is visible on top of the rare earth element oxide "cake," where terbium and dysprosium were the main REEs collected. The enrichment of the final cake was approximately 1.8% total REE.

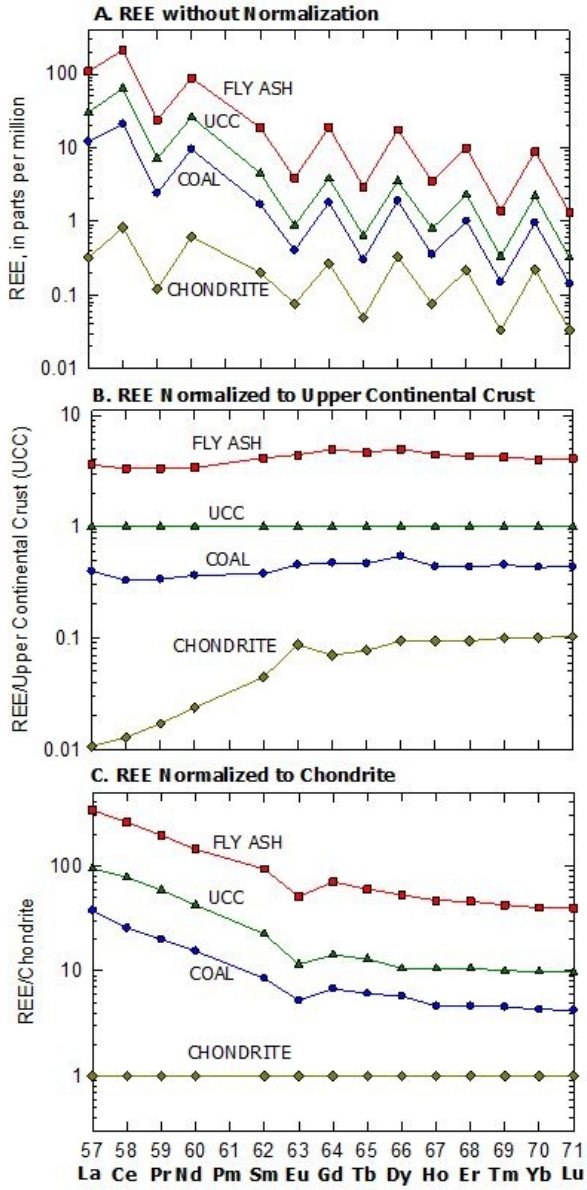

Figure 1. Plots showing how REE data are represented, including distributions for: 1) fly ash from a Kentucky power station burning Appalachian Basin Fire Clay coal (fly ash), data from Taggart et al. (2016); 2) the upper continental crust (UCC), data from Taylor and McLennan (1985); 3) U.S. coal in USGS COALQUAL database (coal), data from Finkelman (1993); and 4) chondrite normalizing values (chondrite), as suggested by Korotev (2009). Plots show how normalization of REE concentration data results in smooth patterns for distribution for elements plotted in order of atomic number.

A. REE concentration data in parts per million showing a sawtooth pattern with even-atomic-numbered elements (Ce, Nd, Sm, Gd, Dy, Er, and Yb) more abundant than odd-numbered elements (Pr, Eu, Tb, Ho, Tm, and Lu) due to the Oddo-Harkins effect. Promethium (Pm, atomic number 61) is omitted because it is not stable in nature.

B. REE normalized to upper continental crust (UCC). Plot shows that REE distribution of fly ash and coal nearly parallel UCC, with greatest REE enrichment in fly ash. REE in coal are less than in UCC.

C. REE normalized to chondrite showing similar patterns for fly ash, UCC, and coal, with each showing enrichment in light rare earths relative to chondrite. The prominent dip in the patterns at europium (Eu,

atomic number 63), is a europium anomaly (see text). Chondrite lacks this Eu anomaly. A chondrite-normalized plot is used later in this chapter.

111x213mm (96 x 96 DPI)

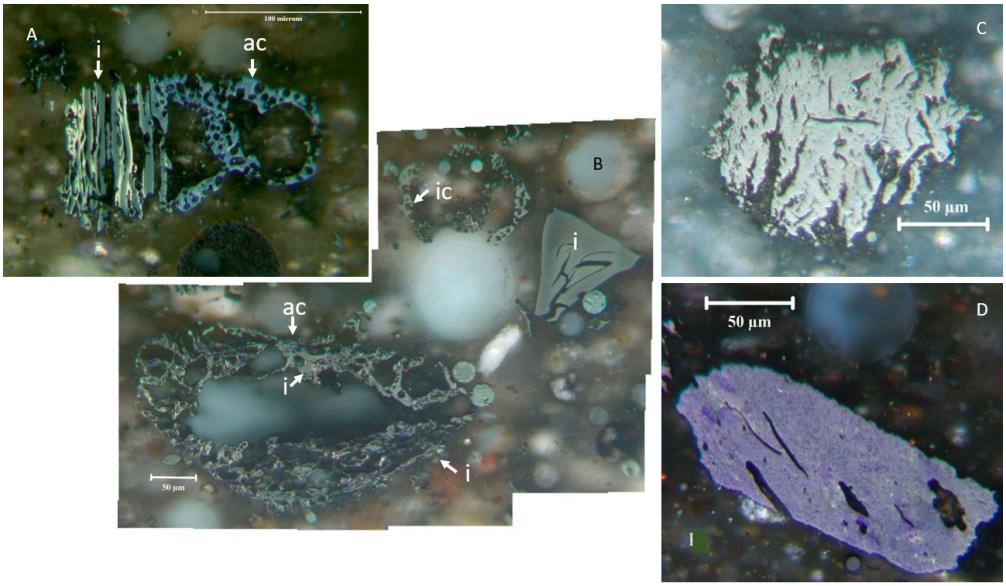

Figure 2. Coal-derived carbons from the combustion of Eastern US bituminous coals. A/ Inertinite (i) and anisotropic coke (ac). Image MD PR 01. B/ Inertinite (i), isotropic coke (ic), and anisotropic coke (ac). Image 93902 11.
C/ US San Juan Basin subbituminous coal-derived char. Image 92922 04 from Hower et al. (2017a).
D/ Chinese Yunnan anthracite-derived carbon. Image Yunnan 2 02 from Silva et al. (2012).

341x197mm (96 x 96 DPI)

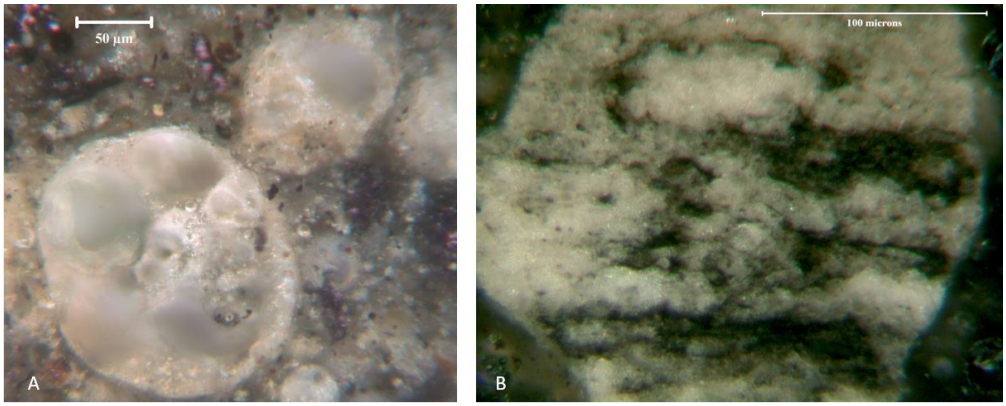

Figure 3. Glassy fly ash particles from the combustion of Eastern US bituminous coals. A/ Glass cenospheres. Image 93685 06. B/ Particle with glass and dark, partially vitrified shale or silt bands. Image MD PS 10.

319x127mm (96 x 96 DPI)

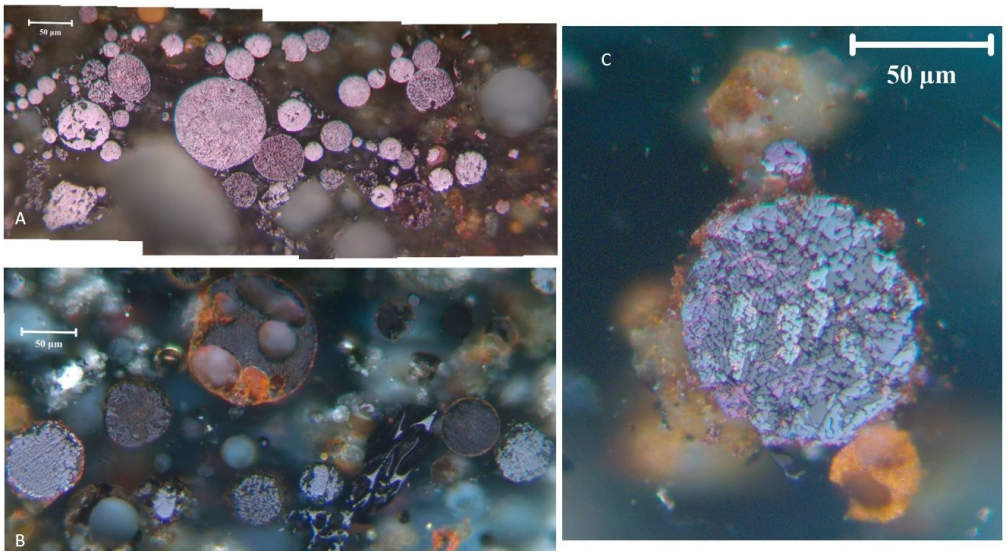

Figure 4. Spinel minerals from the combustion of Eastern US bituminous coals. A/ Spinel forms in a bottom ash. Image 93662 01. B/ Spinels in fly ash. Image 93614 04. C/ Spinel from a bottom ash. Image 93933 08.

348x190mm (96 x 96 DPI)

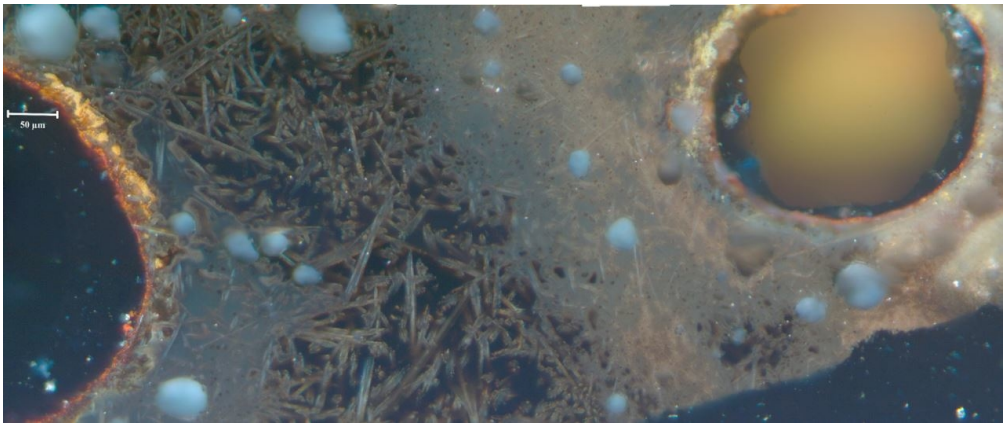

Figure 5. Stoker combustion ash from the burning of Eastern US bituminous coals. Much of the left portion of the image, the triangular lower right areas, and the "bubble" in the upper right are void spaces. Much of the rest of the particle is packed with varying densities of mullite crystals in a glassy matrix. The left, rounded edge of the particle has an oxidation rim. Image 93962 06 from Hower et al. (2018a).

337x141mm (96 x 96 DPI)

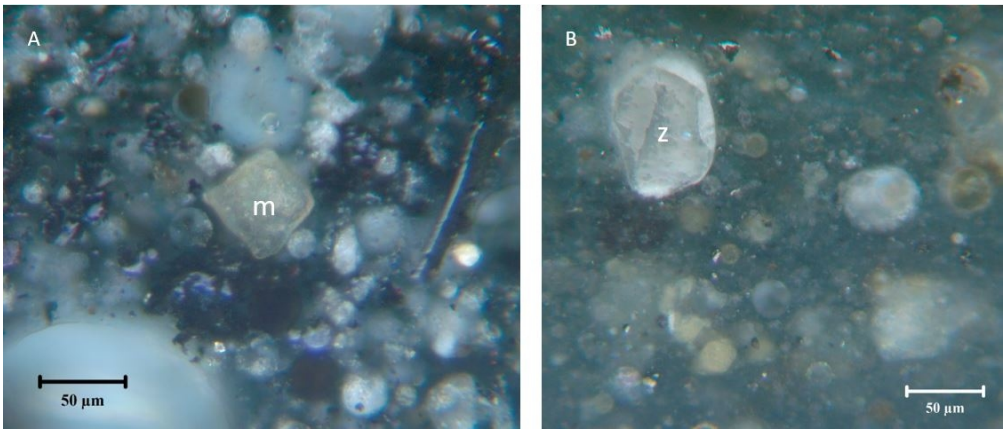

Figure 6. A/ Monazite (m) with glassy particles in an Eastern US bituminous coal-derived fly ash. Image 93954 04 from Hood et al. (2017). B/ Zircon (z) in fly ash from Powder River Basin subbituminous coal-derived fly ash. Image 93971 02.

297x126mm (96 x 96 DPI)

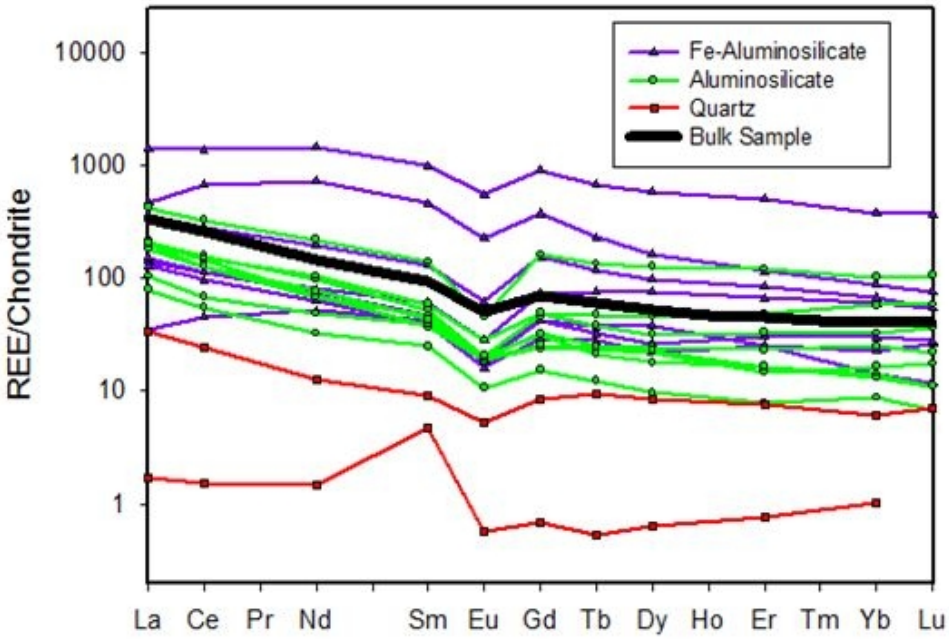

Figure 7. Chondrite-normalized plot of SHRIMP-RG results for constituents of a fly ash sample derived from Appalachian Basin Fire Clay coal. Figure is modified after Kolker et al. (2017). Bulk REE distribution (heavy solid line) is from Taggart and others (2016). Plot demonstrates the relative enrichment of REE in Fe-bearing aluminosilicate glass relative to Fe-poor glasses. Quartz shows relative REE depletion or is below detection. Promethium (Pm, atomic number 61) is omitted because it is not stable in nature.

145x101mm (96 x 96 DPI)

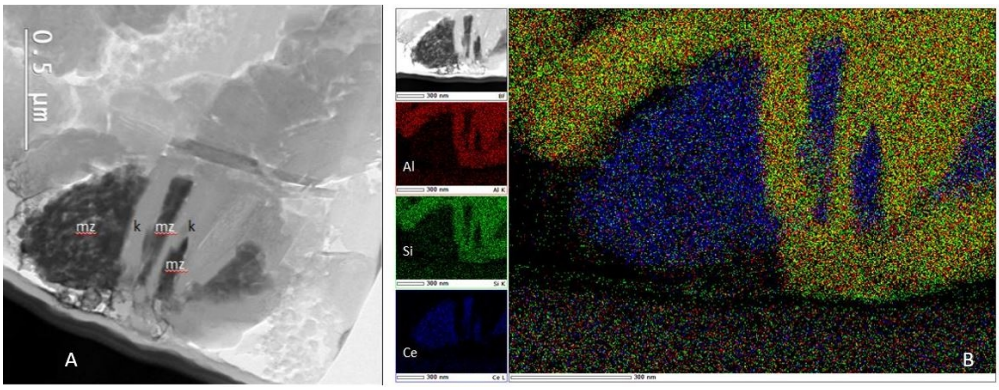

Figure 8. A/ Mixed monazite (mz) and kaolinite (k) grain in Fire Clay coal. B/ The EDX scan shows the segregation of the kaolinite (Al and Si) from the monazite (using Ce as a proxy for the REE in monazite). After Hower et al. (2018c).

307x118mm (96 x 96 DPI)

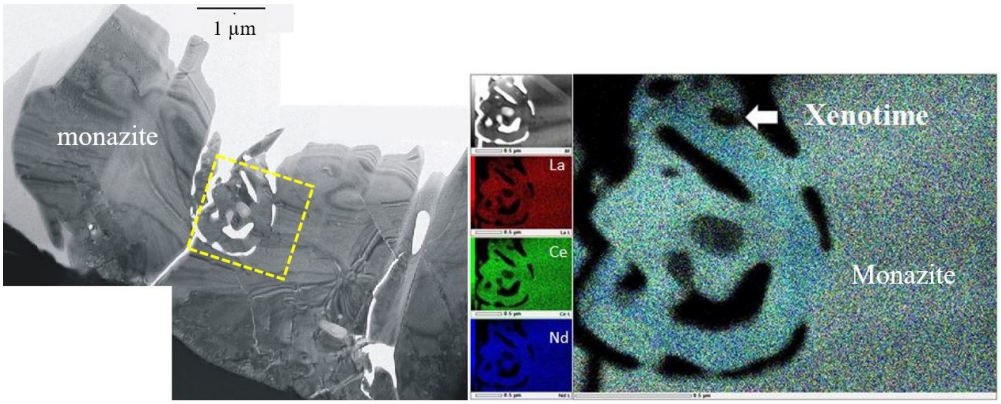

Figure 9. Monazite with included xenotime in the fly ash from the combustion of an Eastern US bituminous coal blend. After Hower et al. (2017b).

334x132mm (96 x 96 DPI)

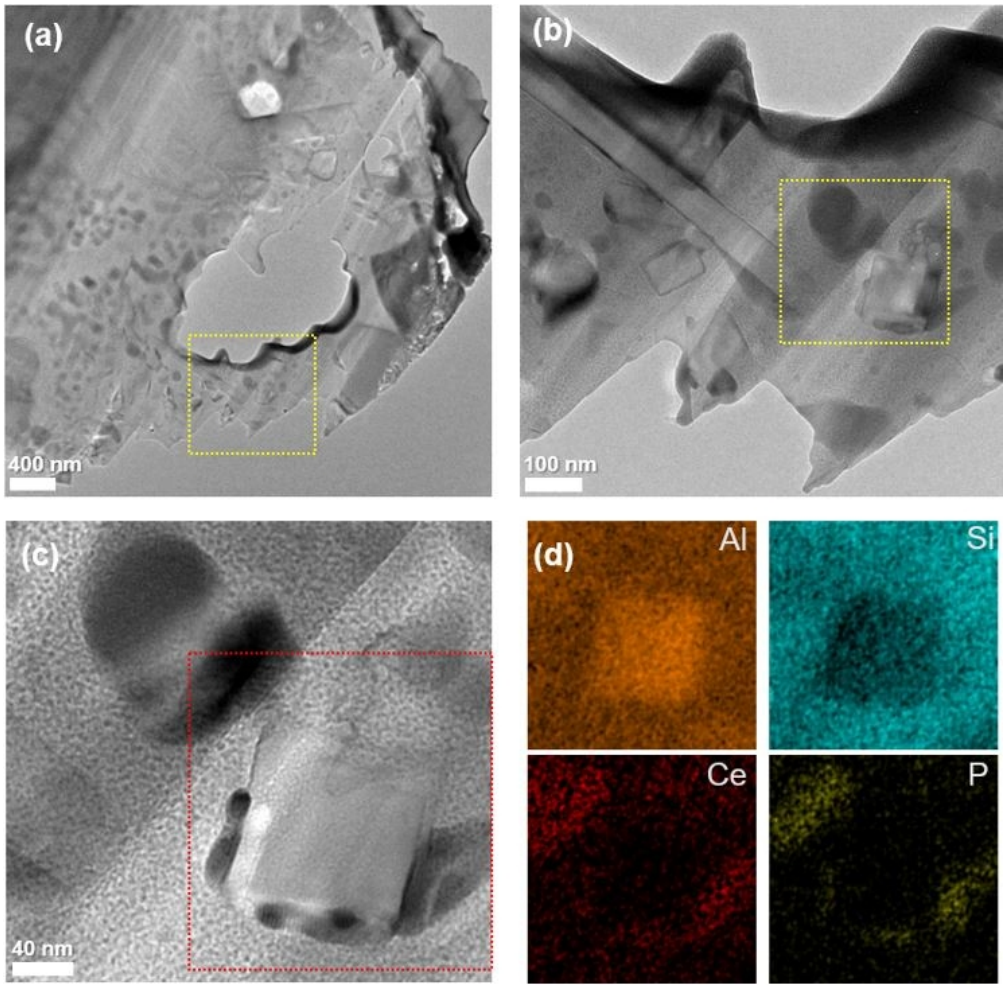

Figure 10. Ce-phosphate on mullite in stoker ash from the combustion of an Eastern US bituminous coal blend. After Hower et al. (2018a).

196x192mm (96 x 96 DPI)

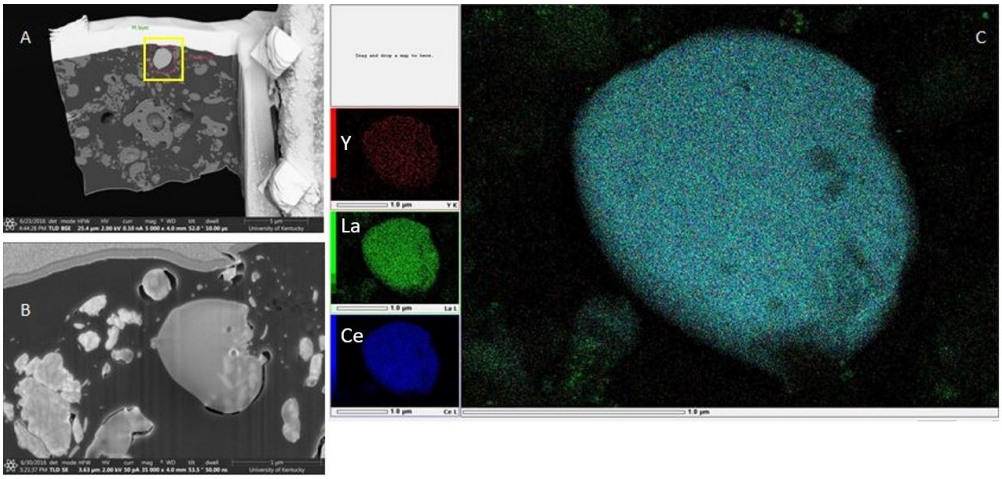

Figure 11. Opposing sides and different sizes of the FIB liftout slice (A & B). C/ EDX image for Y, La, and Ce showing the diffuse nature of the REE distribution. From Hood et al. (2017).

336x160mm (96 x 96 DPI)

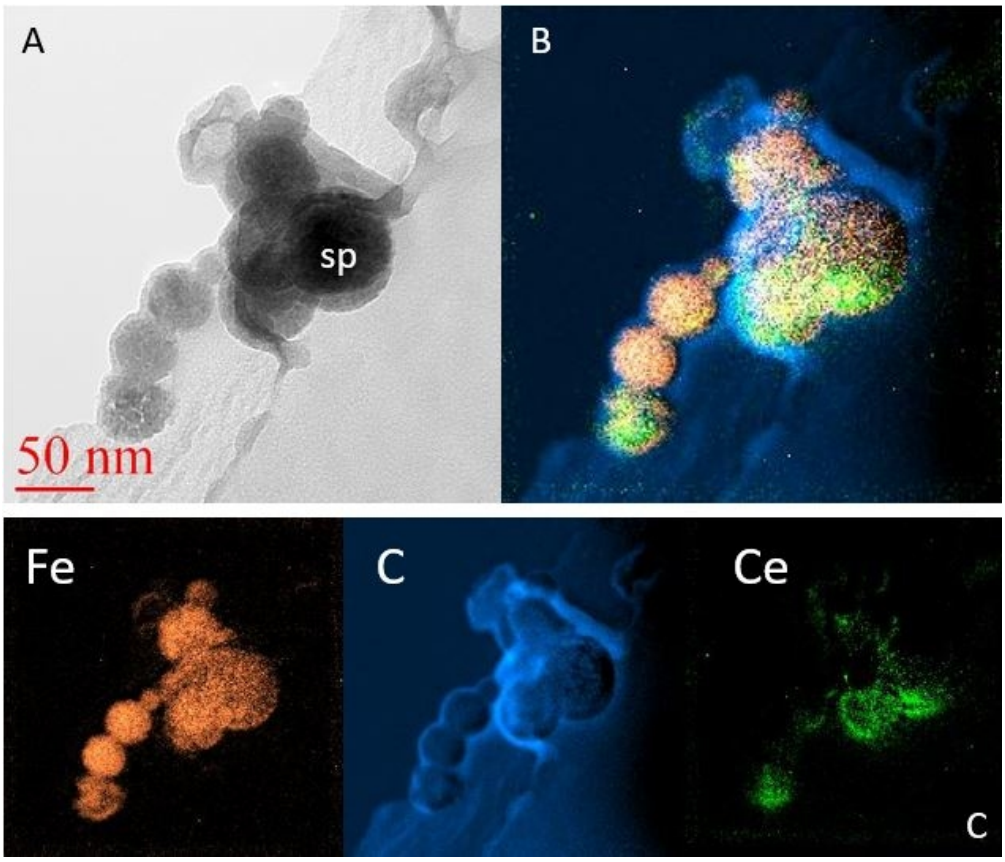

Figure 12. A/ TEM image of Fe-spinel minerals (sp) in fly ash from the combustion of an Eastern US bituminous coal blend. B/ Composite EDX image based on the elements mapped individually in (C). After Hower et al. (2017b).

167x142mm (96 x 96 DPI)

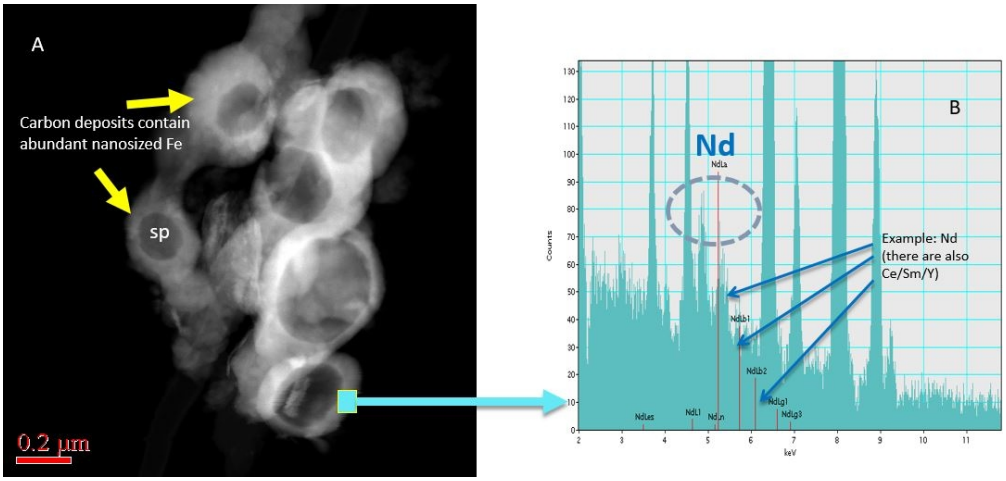

Figure 13. A/ TEM image of spinel (sp) surrounded by carbon. The area scanned by EDX is shown by the rectangle on the lower right of (A). The fly ash is from the combustion of an Eastern US bituminous coal blend. B/ EDX scan of area shown on (A), indicating that the carbon deposit on the surface of the spinels includes/entrains Nd, Ce, Sm, and Y. After Hower et al. (2017b).

285x135mm (96 x 96 DPI)

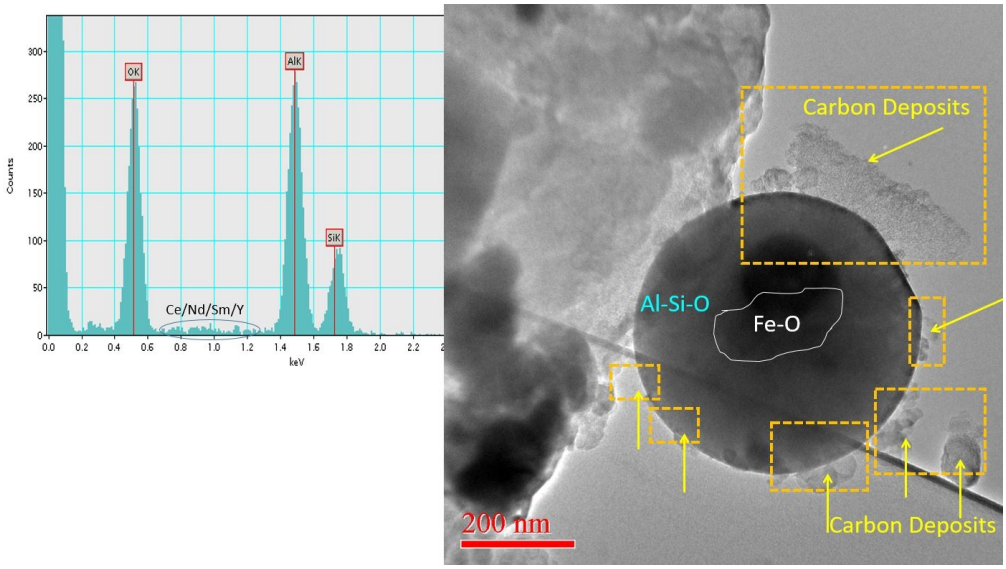

Figure 14. High resolution TEM image (right) of Al-Si glass sphere surrounded by graphitic carbon deposits. The fly ash is from the combustion of an Eastern US bituminous coal blend. The composite of 50 EDX scans (left) indicates that the carbon contains Ce, Nd, Sm, and Y. After Hower et al. (2017b).

369x206mm (96 x 96 DPI)

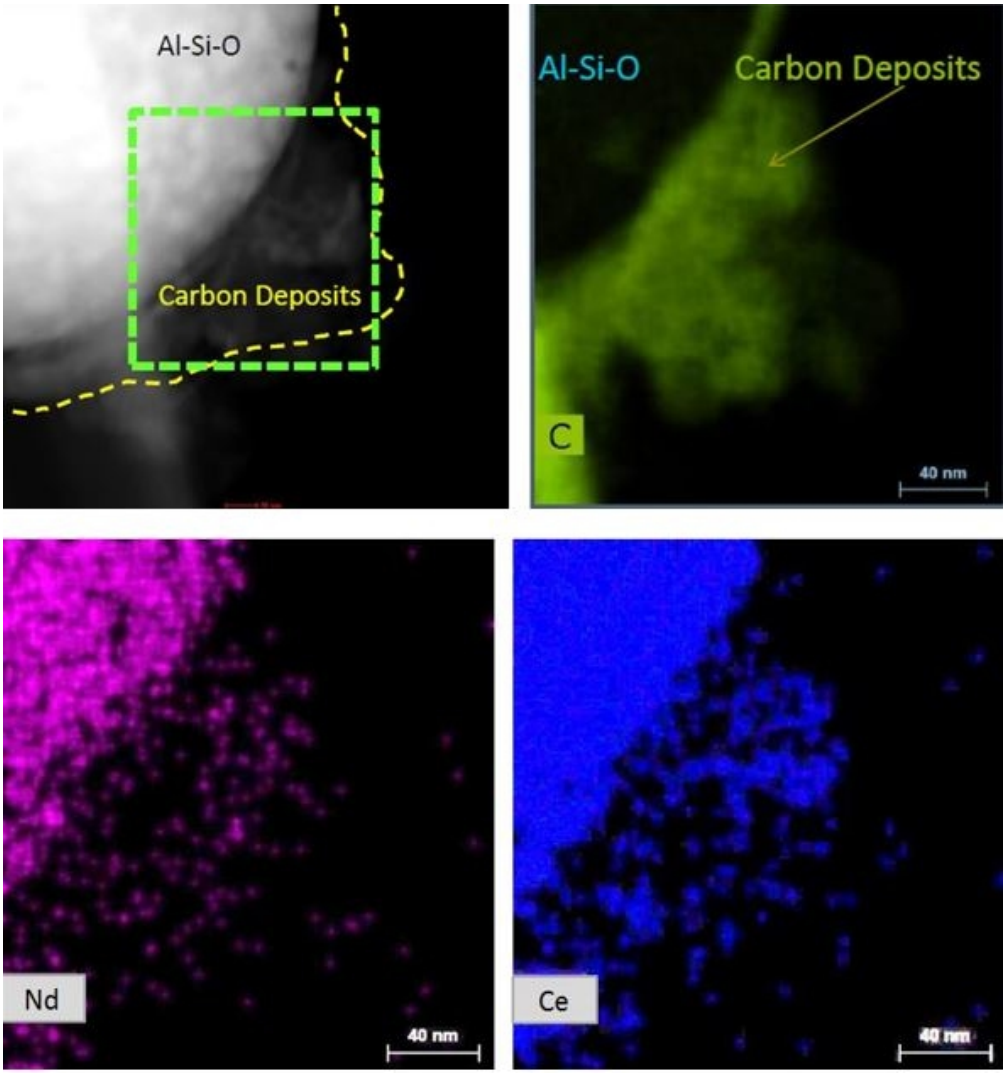

Figure 15. High resolution TEM image (upper left) of Al-Si glass sphere surrounded by graphitic carbon deposits. EDX images of C, Nd, and Ce are shown in the upper right, lower left, and lower right images, respectively. The EDX C overlapping the Al-Si glass is blacked out on the upper right image, concealing the basis for the dense Nd and Ce concentrations coincident with the glass. The fly ash is from the combustion of an Eastern US bituminous coal blend. After Hower et al. (2017b).

156x166mm (96 x 96 DPI)

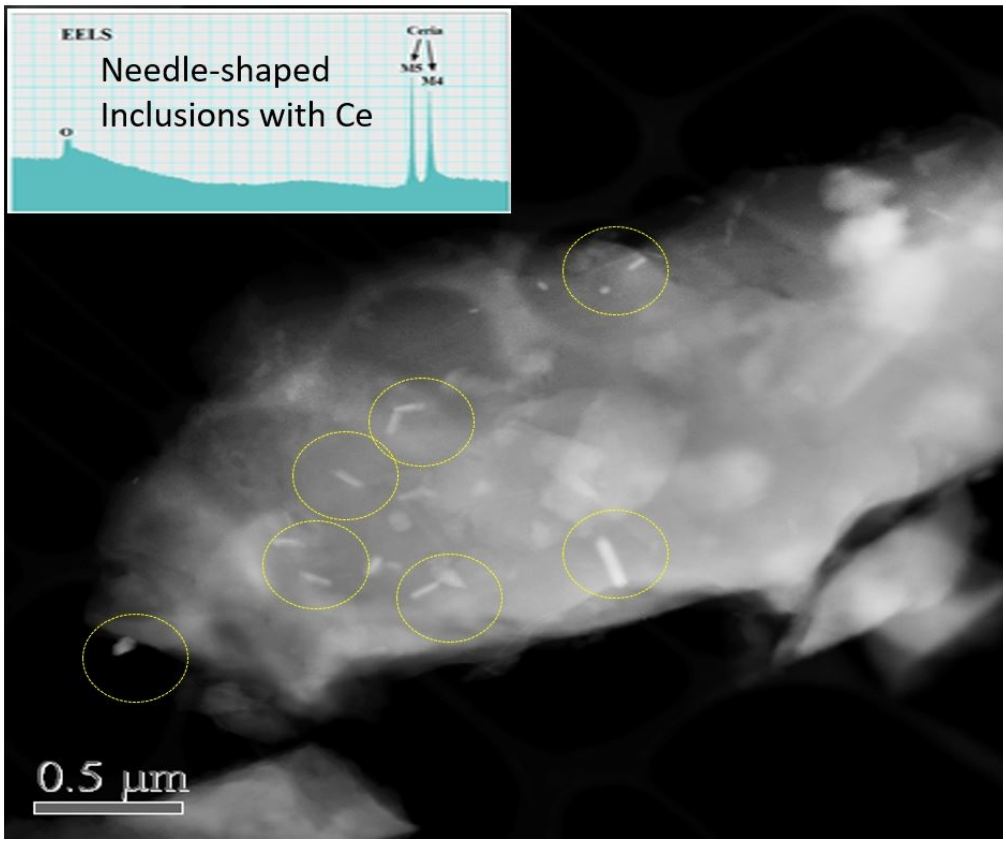

Figure 16. EELS imaging indicating the presence of Ce associated with needle-shaped minerals (in circles). The fly ash is from the combustion of an Eastern US bituminous coal blend. After Hower et al. (2017b).

246x206mm (96 x 96 DPI)

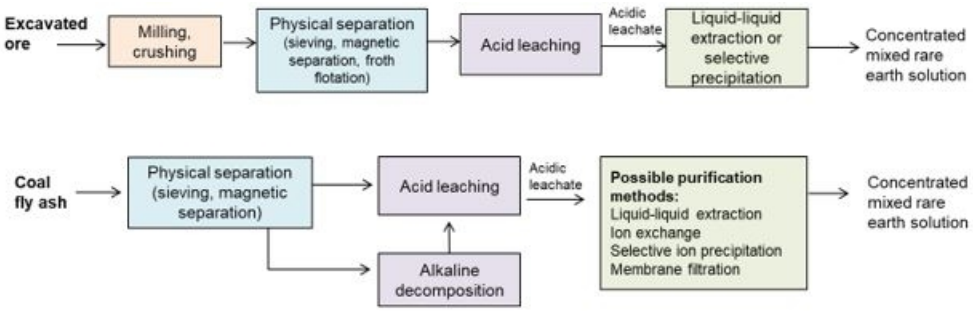

Figure 17. Example sequence of unit processes for the recovery and separation of rare earth elements at conventional mining operations (top schematic) and potential modifications to the recovery process for REE-enriched coal fly ash (bottom schematic).

165x51mm (96 x 96 DPI)

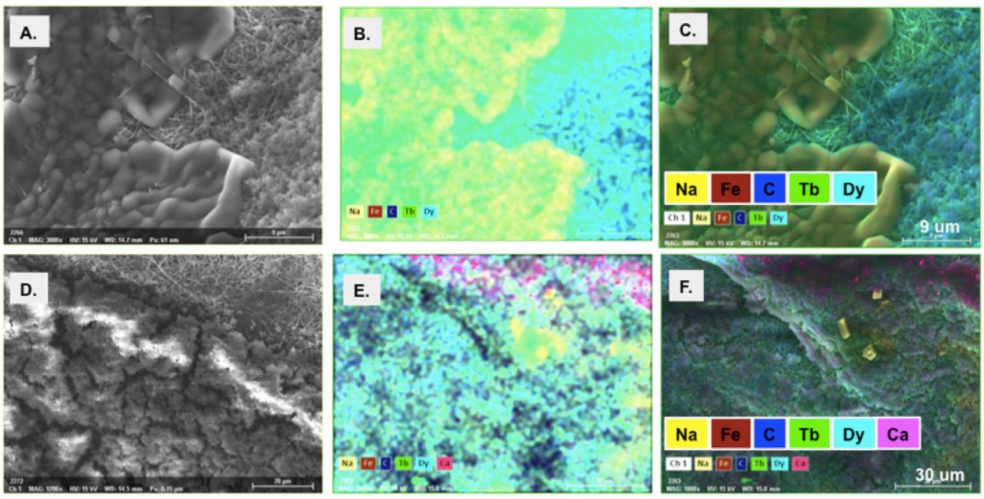

Figure 18. Scanning electron micrograph with energy dispersive x-ray spectroscopy (SEM-EDS) of rare earth elements separated from coal ash leachate using electrochemical deposition on carbon nanotube filters. Pre-treatments included an alkaline sintering of the coal ash, followed by a nitric acid extract and a pH titration using sodium hydroxide. Residual sodium is visible on top of the rare earth element oxide "cake," where terbium and dysprosium were the main REEs collected. The enrichment of the final cake was approximately 1.8% total REE.

165x83mm (220 x 220 DPI)

Table 1. Rare earth elements in coal fly ash that could be analyzed for bulk speciation by X-ray absorption spectroscopy and potential interfering elements to consider in coal fly ash. The concentration values (from Taggart et al., 2016) correspond to fly ashes generated from coals of the central Appalachian basin in the U.S. (generally the more enriched of U.S. coal fly ashes). Fly ash samples are also enriched in other elements with absorption or emission energies that could interfere with the target element energies (Kortright and Thompson, 2009; Williams, 2009).

Element	**Concentration in fly ash**	**Absorption energy**	**Emission energy**	**Potential interfering elements**
Cerium (Ce)	100 – 200 mg kg^{-1}	5732 eV (L_3-edge)	4840.2 eV ($L\alpha_1$)	V, Ba
Lanthanum (La)	70 – 110 mg kg^{-1}	5483 eV (L_3-edge)	4651.0 eV ($L\alpha_1$)	Ti
Neodymium (Nd)	60 – 90 mg kg^{-1}	6208 eV (L_3-edge)	5230.4 eV ($L\alpha_1$)	Possibly Ce
Yttrium (Y)	80 – 100 mg kg^{-1}	17038 eV (K-edge)	14958 eV ($L\alpha_1$)	None likely